Anchoring a Molecular Iron Based Water Oxidation Catalyst onto a Carbon Paste Electrode

Marcus Byström

KTH Chemical Science
and engineering

Master's Thesis

Stockholm 2015

Abstract

This thesis concerns the development and the study of Iron-based water oxidation catalysts (WOCs) and how to immobilize them onto the hydrophobic surface of a carbon paste electrode. In the introductory chapter a general background of the field of water splitting and this thesis is given. In the second chapter, experimental performance is described from synthesis to measurements of a complete complex-doped electrode. The third chapter deals with the results and the discussion of the performed experiments. In chapter four, a descriptive conclusion of the obtained data is held.

Sammanfattning

Det här arbetet berör studien och utvecklingen utav järnbaserade katalysatorer, speciellt framtagna för för delning utav vatten. Utöver detta undersöks även om dessa katalysatorer (WOCs) kan immobiliseras på den hydrofoba ytan hos elektroder gjorda på kol-pasta. I det inledande kapitlet ges en generell bakgrund till området som berör delning utav vatten. I det andra kapitlet presenteras det experimentella utförandet utav synteser samt elektrokemiska mätningar som berörts under arbetets gång i jakten på en komplexdopad elektrod. I det tredje kapitlet diskuteras resultaten från mätningarna samt möjliga framtidsutsikter. I det fjärde kapitlet presenteras slutsatserna utav studien.

Keywords: Iron Catalyst, Water Oxidation, Electro Chemistry, Carbon Paste Electrode, Water Splitting.

Abbreviations

ΔG	Gibbs free energy of activation
ATP	adenosine triphosphate
bda	2,2'-bipyridine-6,6'-dicarboxylic acid
bdpmcn	N,N-bis(2-methyl-4-dodecoxypyridyl)-N,N-dimethylcyclohexyldiamine.
bcdpmcn	N,N-bis(2-carboxamide-4-dodecoxypyridyl)-N,N-dimethylcyclohexyldiamine
bpdcn	N,N-bis(2-methylpyridyl)-N,N-didodecylcyclohexyldiamine.
bpmcn	N,N-bis(2-methylpyridyl)-N,N-dimethylcyclohexyldiamine.
bpy	2,2'-bipyrimidine
dmso	dimethyl sulfoxide
Ce^{IV}	$Ce(NH_4)_2(NO_3)_6$
CPE	carbon paste electrode
CV	cyclic voltammetry
DCE	1,2-dichloroethane
DCM	dichloromethane
ESI	electron spray ionization
ESR	electron spin resonance
HPLC	high performance liquid chromatography
I2M	interaction of two M-O units
LUMO	lowest unoccupied molecular orbital
MSD	mass selective detector
MS	mass spectrometry
$NADP^+$	nicotinamide adenine dinucleotide phosphate (oxidized)
NADPH	nicotinamide adenine dinucleotide phosphate (reduced)
NHE	normal hydrogen electrode
NMR	nuclear magnetic resonance
OEC	oxygen evolving complex
PCET	proton-coupled electron transfer
PSI	photosystem I
PSII	photosystem II
RT	room temperature
RuBisCO	ribulose-1,5-bisphosphate carboxylase/oxygenase
TAML	tetra amido macrocyclic ligand
TLC	thin layer chromatography
UV	ultra violet
WNA	water nucleophilic attack
WOC	water oxidation catalyst

Table of Contents

1 Background and Theory

1.1 Introduction

The chemical reaction in which water molecules decompose into hydrogen gas (H_2) and oxygen (O_2) is commonly referred to as water splitting. Different systems designed to split water and to generate hydrogen gas for a future hydrogen economy have already been invented but so far none of them are able to compete with the more economically favorable energy production from natural gas and oil.

In nature, plants, algae and cyanobacteria harvest sunlight and use it in their photosynthesis together with water to produce ATP and NADPH for their cellular growth and synthesis of carbohydrates. The idea of utilizing the sun as an energy source and water as a source of electrons and protons has inspired scientists all over the world to create an artificial water splitting system as a carbon-neutral source of energy. The total process of artificial water splitting (Equation 1) can be divided into two half reactions: the oxidation of water (Equation 2) and the reduction of protons (Equation 3)[1].

Equation 1 $2\mathrm{H_2O} + h\nu \rightarrow 2\mathrm{H_2} + \mathrm{O_2}$
Equation 2 $2\mathrm{H_2O} \rightarrow \mathrm{O_2} + 4\mathrm{H^+} + 4\mathrm{e^-}$
Equation 3 $2\mathrm{H^+} + 4\mathrm{e^-} \rightarrow \mathrm{H_2}$

Out of the two half reactions, the oxidation of water is the more energy demanding and is often seen as a bottleneck for the whole water splitting process. Multiple proton-coupled electron transfer (PCET) processes together with the bond formation of O_2 is what makes water oxidation so complex and thermodynamically unfavorable. To increase the reaction rate and minimize the required over potential, a water oxidation catalyst (WOC) can be added to the system. If a catalyst was to be used in a large scale industrial process there are some criteria it must uphold: (i) long-term stability, (ii) high activity, (iii) working at a low over potential, (iv) nontoxic properties, (v) economically favorable. Yet of today no molecular WOC has shown properties required for large scale application[2] but mechanistic and device studies on the topic are being carried out to guide chemists into a more effective WOC and device design.

The novel concept of this work is to retailor a previously tested system, with a catalyst previously anchored onto solar-responsive WO_3 electrodes, to a new system where a similar catalyst will be anchored onto an electrode with a hydrophobic surface. Even though exciting, this concept brings forth a number of challenges; (i) changing too much of the structure may impinge on the activity of the WOC, (ii) the synthesis of the complex will have to change which might affect reaction yield and therefore the cost of the complex, (iii) changing the whole system will not only influence on the properties of the catalyst but may also change the mechanisms and kinetics of the total device including electrode and electrolyte.

1.2 The water oxidation catalyst of Photosystem II

Adenosine triphosphate (ATP) is a nucleotide that plays a central role in the energy management of the cell. It serves as a carrier of chemical energy within the cells and is used by structural proteins and enzymes in numerous cellular processes, including motility, biosynthetic reactions and cell division. In plant cells, a process called the Calvin cycle[3] uses ATP together with NADPH[i] and a catalyst called RuBisCO to synthesize carbohydrates from CO_2. These reactions occur in the fluid filled area of the chloroplasts[ii] called the stroma, just outside the thylakoid membranes. The vital energy carriers ATP and NADPH are both generated in a process called the photosynthesis in plant cells, presented in Figure 1.

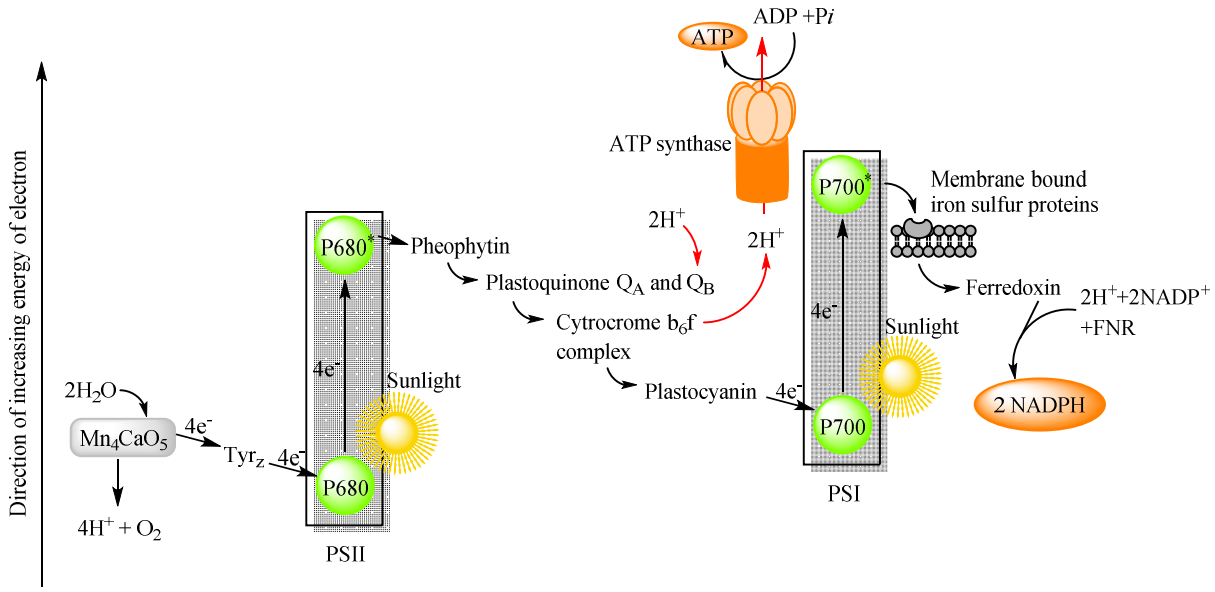

Figure 1. The Z-scheme diagram of photosynthesis.

The photosynthesis starts in photosystem II (PSII) with the excitation of electrons in a reaction center of chlorophyll labeled P680. The exited species P680* will then lose one electron to pheophytin, producing oxidized P680 ($P680^+$) and reduced pheophytin ($Pheo^-$). $Pheo^-$ will then pass on the electron to the reaction center Q_A of the protein complex plastoquinone. Plastoquinone Q_A will then pass on the electron to the neighboring plastoquinone Q_B. When Q_B has accepted two electrons from Q_A, it will start to form bonds with two free protons from the stroma. As the hydrogen bonds are formed, Q_BH_2 will detach from its protein binding site and diffuse through the hydrophobic channels of the thylakoid membrane to the cytochrome b_6f complex situated in the lumen. Cytochrome b_6f oxidizes Q_BH_2 to Q_B with the release of the two protons causing pH to drop in the lumen. The obtained proton motive force over the thylakoid membrane is used to power the synthesis of ATP with ATP synthase and the two building blocks ADP and phosphate (Pi). The abstracted electron of cytochrome b_6f is then passed on to a copper-containing protein called plastocyanin. Plastocyanin will then in turn distribute electrons to the oxidized electron donor of photosystem I (PSI), chlorophyll $P700^+$. The reason to why PSI starts with oxidized $P700^+$ is that when sunlight hits the

[i] A biological reducing agent found in eukaryotes as well as in prokaryotes.
[ii] This is the organelle responsible for the photosynthesis in plants.

chloroplasts of the plant, both chlorophyll P680s and P700s electrons excite concurrently. In PSI, immobile membrane bond iron sulfur proteins will abstract the excited electrons of P700* and generate the previously mentioned oxidized species $P700^+$. The more mobile iron sulfur protein, ferredoxin, will in turn abstract the electrons and form a reduced ferredoxin species. Together with the enzyme ferredoxin-NADP oxidoreductase and free protons, the reduced ferredoxin can reduce $NADP^+$ to NADPH.

In order for the plant cell to further produce ATP and NADPH, the oxidized chlorophyll $P680^+$ in PSII has to obtain an electron and relax back to P680. Nature has solved it so that the highly reactive $P680^+$ rapidly oxidizes a tyrosine-Z to a milder tyrosine-Z radical species and relaxes back to P680. The tyrosine-Z radical will then extract electrons from a nearby Mn_4CaO_5 protein complex, often referred to as the oxygen evolution complex (OEC), which in turn will oxidize adjacent water molecules to form H^+ and O_2. The redox reactions of the OEC are often referred to as the KoK Cycle[4] which is a widely accepted theory from 1970 that the protein complex exists in 5 different oxidative states, as illustrated in Figure 2.

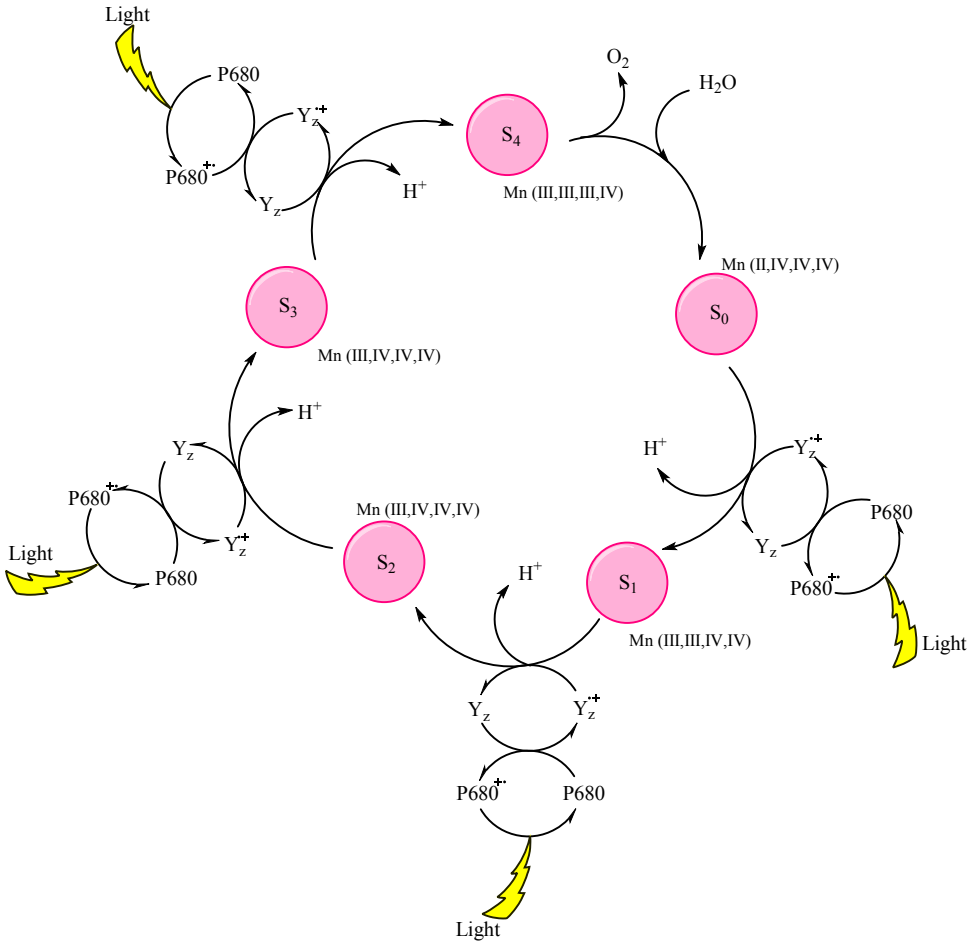

Figure 2. KoK cycle with OEC Mn_4CaO_5.

Clear crystal structures of the OEC has been reported[5-8], but the full understanding of how the electron transport chain mechanisms works is yet not profound, making this a hot topic for biochemists around the world.

Solving the ongoing debate could also be valuable in the field of artificial water splitting. Better understanding of the mechanisms of the OEC could be applied in the development of artificial water oxidation complexes and hopefully pave the way for devices able to compete with the energy production from the petroleum industry.

1.3 Synthetic water oxidation catalysts

The OEC of photosystem II with its strong electron donating oxo- and carboxylate ligands has a stable and high valent Mn center with low redox potential, properties sought in every water oxidation catalyst (WOC). Its ligand structure and properties has inspired chemists to synthesize transition metal WOCs of their own.

Even though the Mn-OEC found in nature is performing well, scientists have had hardships synthesizing high performing Mn-based WOCs. Only a few cases of Mn catalysts capable of performing water oxidation have been reported[iii]. Crabtree and Co-workers[9] discovered the first family of Mn WOCs **(1**; Figure 3**)** but it wasn't until Yagi and coworkers[10] invented a method to absorb **1** on montmorillonite K10, Kaolin and mica that the catalyst could be classified as a real WOC. With the use of Ce^{IV} as a sacrificial oxidant, **1** was able to successfully mediate water oxidation with a TON of 17 without the use of an oxygen transferring oxidant.

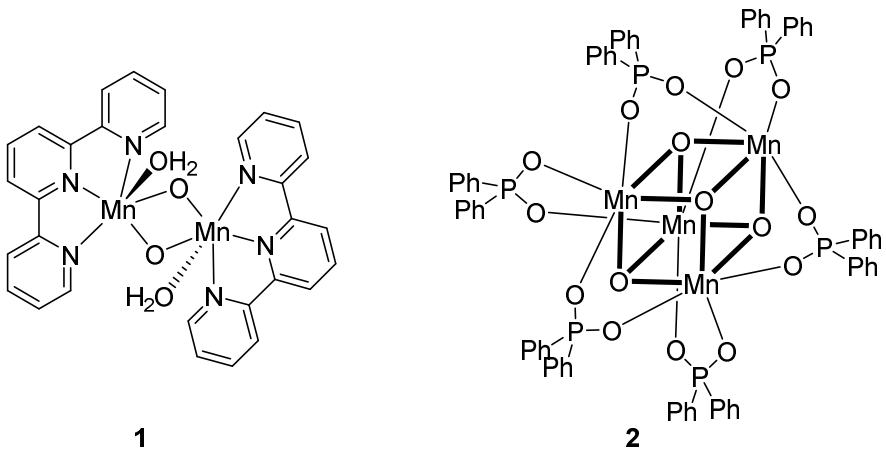

1 **2**

Figure 3. Mn based WOCs.

Complex **(2**; Figure 3**)** belongs to the second family of Mn-complexes able to perform water oxidation and was discovered by Dismuke and co-workers[11]. The Dismuke group proved that if **2** was irradiated with UV light, the complex could release one mole of oxygen per mole of catalyst via the intermolecular O-O coupling of the two manganyl oxoes. **2** was thereafter tested for its electrochemical water oxidation property on a conducting Nafion electrode, showing a turn over number[iv] (TON) of 1000.

Not only Mn has been used as center metal in water oxidation complexes. In 1982, T.J. Meyer and co-workers reported the first molecular ruthenium catalyst[12], cis,cis-$[(bpy)_2(H_2O)Ru^{III}ORu^{III}(OH_2)(bpy)_2]^{4+}$ (**3**, Figure 4), for water oxidation which would be the stepping stone for future research on the topic.

The catalyst of today with the highest TON belongs to the ruthenium complex family and was discovered by Lichen Sun and co-workers[13]. The WOC is a ruthenium-bda (bipyridine-dicarboxylate) complex (**4**; Figure 4) capable of performing more than 10^5 turnovers.

[iii] A Mn based WOC using oxygen transferring oxidants is not considered as a real WOC and therefore not brought up here.

[iv] The number of catalytic cycles the catalyst is able to perform before decomposition.

A drawback of the ruthenium catalysts is their high cost. Being one of the rarest elements in the earth's crust[14] makes mining and refining it a challenging job, resulting in an appurtenant high prize. The criterion of a cheap water oxidation complex is therefore hard to meet with the use of ruthenium as the metal center of the WOC.

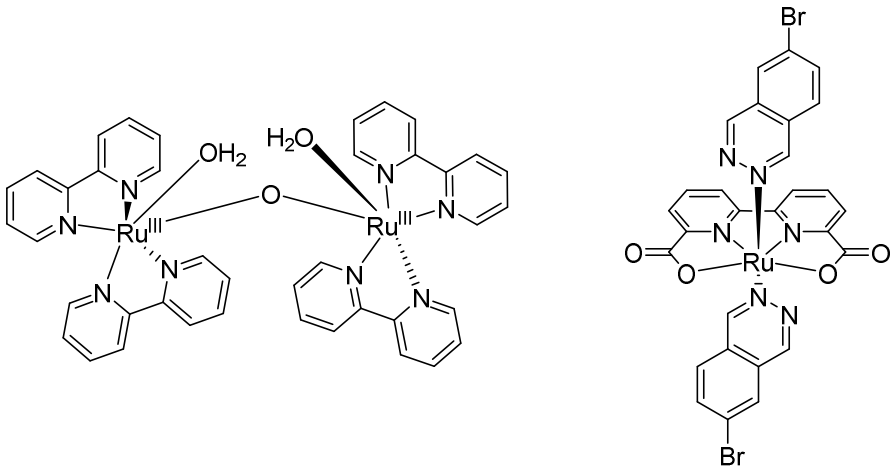

3 **4**

Figure 4. Ruthenium bda complex.

Beside ruthenium and manganese, other transition metal WOCs such as iridium[15-18], cobalt[19-21], osmium[22], copper[23-24] and iron[25]-based, have been reported to work successfully. The latter mentioned iron based WOCs, contains one of the most abundant elements in the earth´s crust, iron, which potentially could make it more cost efficient than other transition metal complexes. Discovering a well performing iron-centered catalyst could therefore lead to an alternative source of energy, economically able to compete with the fossil fuels.

In 2010, the first Fe^{II} based tetra-amido macrocyclic ligand (-TAML) WOCs (**5**; Figure 5) were discovered by Collins and co-workers. Their work opened up a new chapter in the search for a large-scale affordable WOC.

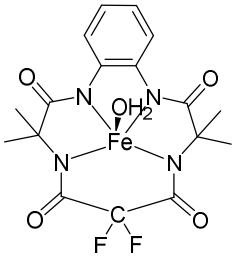

5

Figure 5. Molecular structure of $iron^{II}$-TAML family skeleton.

1.4 Transformation of water to oxygen and hydrogen

The activation energy required to perform a redox reaction is derived from Gibbs free energy (Equation 4) and Nernst equation (Equation 5):

Equation 4 $\Delta G = -nFE$

Equation 5 $E = E°_{cell} - \frac{RT}{nF}\ln(\frac{ox}{red})$

In order to tell if a reaction occurs spontaneous, the Gibbs free energy has to be smaller than zero which indicates that the energy *E* in the Nernst equation has to be positive for a redox reaction not to be endergonic[v].

The total energy of a redox reaction is often considered to be two half reactions where $E=E_{tot}=E_{1/2}(ox) - E_{1/2}(red)$. If $E_{1/2}(ox)$ increases, and or $E_{1/2}(red)$ decreases, the total energy of the reaction will increase resulting in a more energetically favored reaction with a lower ΔG.

When illustrating reduction and oxidation of different species, a so called Pourbaix diagram can be helpful. The first half reaction of water splitting, the oxidation of water, has activation energy so high that it doesn't occur spontaneously at standard ambient temperature and pressure.

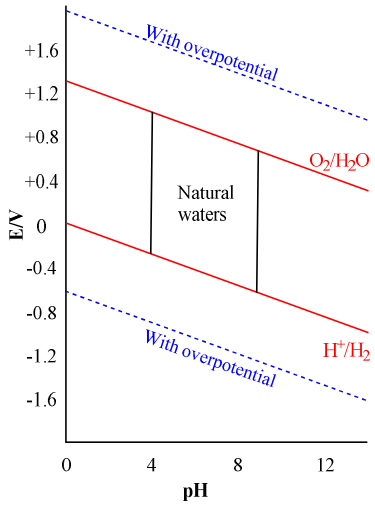

Figure 6. Pourbaix diagram of water oxidation and proton reduction.

Illustrated in the Pourbaix diagram (Figure 6), by the upper red curve, a standard reduction potential of more than 1.23 V is required when using the normal hydrogen electrode (NHE) in order to surpass the energy barrier of activation at pH 0 for the oxidation of water. The other half reaction of water splitting, the reduction of protons, occurs at a standard reduction potential of 0 V illustrated as the lower red line in the diagram. The total redox potential for water splitting is therefore $E_{tot}= E°_{1/2}(ox)-E°_{1/2}(red)$ =-1.23V-0V=-1.23V. Thus, the required energy for the water splitting process deduced from Equation 5 is ΔG°=237.4kJ for every mole of reacted water. The positive sign of the answer corresponds to a positive ΔG and a non-spontaneous reaction. If the pH increases, the redox

[v] An endergonic reaction is a non-spontaneous reaction.

potential for the water oxidation decreases and the $E°_{1/2}$(ox) is decreased. At the same time $E°_{1/2}$(red) is lowered and since both half reactions are linearly dependent the decrease in $E°_{1/2}$(ox) will be the same as the decrease of $E°_{1/2}$(red) which corresponds to an unchanged total energy for the whole system and will therefore not change the ΔG°.

To improve the efficiency of an electrochemical reaction, a so called electrocatalyst can be added to the system. As previously mentioned, the more general term for a catalyst specially designed for water splitting is referred to as a WOC. The WOC function at the surface of an electrode or as the electrode surface itself and can either be homogenous or heterogeneous. As a catalyst the typical WOC assists in the indirect electron transfer between water and electrode. By facilitating the intermediate chemical transformation of the WOC and the coordination of water, the overall oxidation reaction can be carried out at a lower over potential.

To facilitate the electron transfer from water to catalyst, one option is to introduce strong electron donating properties to the ligand structure or substituents which will decrease the oxidation potential of the catalyst. If a proton-coupled electron transfer (PCET) reaction is involved, introduction of intramolecular proton acceptors can further enhance the electrochemical process. Another aspect that has to be considered when designing a WOC is the oxidizing power of the catalyst. The stronger oxidizing properties of the catalyst, the more favorable the redox reaction will become. Accordingly, in order to acquire a catalytically operating species with high activity, the redox potential of the WOC must be kept as low as possible in order to favor the electron transfer, but still high enough to maintain the oxidizing power towards water oxidation present. A third consideration that has to be taken into account when designing the WOC is which mechanistic pathway the complex will undergo during the O-O bond formation. The two major accepted pathways are water nucleophilic attack and the two mono radical M-O coupling. For a water nucleophilic attack (WNA), water molecules attack the oxo group of the metal complex in a nucleophilic manner as described in Figure 7. An internal basic site of the complex can here aid in pre-orientation of the water substrate, orienting it into an appropriate angle for attack. To further facilitate the WNA pathway, electron withdrawing groups attached to the ligand will lower the LUMO of the M=O making it more prone to nucleophilic attack. In the interaction of two mono-radical M-O units (I2M), a peroxo intermediate prior to the release of O_2. By reducing the static or steric repulsion and increasing the spin density of the oxo, the coupling between the two M-O species will be favored. As for both WNA and I2M, the release rate of dioxygen is the rate limiting step of both reactions. Several factors could influence on the release rate but up to date there are no clear correlations between electronic effects and the formation of O_2[3].

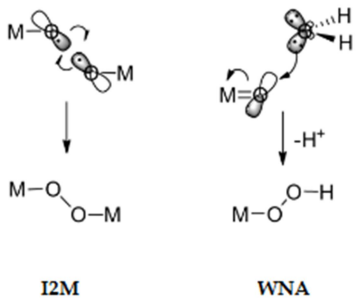

Figure 7. Mechanistic I2M and WNA representations.

1.5 Hydrogen as a fuel

With the recent impoverished situation on oil, renewable substitutes for fossilized fuels have become an increasingly hot subject in both politics and science[26-29]. Hydrogen as a fuel is today most commonly used in electrochemical cells or internal combustion engines with the advantageous property to power vehicles and electric devices without emitting any tailpipe pollutants. Even though hydrogen is the most abundant chemical substance in the universe, its molecular gaseous form H_2 is rarely found in larger quantities around the crust of the earth. The diatomic structure is so light that shortly after being formed it will gain enough velocity from collisions with other gas molecules to eject from the atmosphere of the earth[30].

For this reason, hydrogen initially has to be produced and stored before being accessible and utilizable as a fuel. The scarce amounts of available hydrogen gas will limit its usage in practice to that of an energy carrier like electricity as it isn't a direct harvestable energy resource like oil or coal. This poses an issue because, according to the physical law of the conservation of energy, the production of hydrogen gas will always require more energy than what can be retrieved later on[31]. However, by investing energy into the formation of hydrogen gas, a method to facilitate and store energy for a later purpose can be acquired.

Various methods for hydrogen production have already been invented with the most common ones being production from fossil fuels or water splitting. The dominant form of industrial hydrogen originates from steam reforming[32] where methane and steam reacts endothermically at high temperatures (700-1100 °C) yielding syngas (Equation 6) as a first step[33].

Equation 6 $\mathrm{CH_4 + H_2O \rightarrow CO + 3\,H_2}$

The second step in the steam reforming process is the exothermic water gas shift reaction where the carbon monoxide from previous step reacts with steam at lower temperature (360 °C) yielding more hydrogen gas and carbon dioxide (Equation 7).

Equation 7 $\mathrm{CO + H_2O \rightarrow CO_2 + H_2}$

Even though hydrogen itself is a zero-emission fuel, the side products; carbon dioxide and carbon monoxide are both greenhouse gases which contribute to global warming. This makes steam reforming a questionable option for hydrogen generation from an environmental point of view. Another commonly used method for hydrogen generation is electrolysis of water which has potential to become a more superior option from the environmental point of view. This method can use solar, wind, wave, nuclear and water power along with other energy sources to produce hydrogen from water. The hydrogen generated from electrolysis is also better suited for systems with high purity demands such as for fuel cells with low carbon monoxide tolerance[34].

The general setup for industrial hydrogen production from electrolysis is very similar to that of the Hoffmann voltammeter[35] and uses two platinum electrodes connected to positive and negative terminals of a source of electricity. When current is passed through the system, gaseous oxygen evolution around the anode and hydrogen evolution around the cathode can be observed. Various alternations of the system setup exist[36-37] and many methods have been proven functional, but so far none have proven efficient enough for a future hydrogen economy. If performance of the electrolytic cell devices would be improved, it could lead to a permanent solution of the energy crisis and abatement of greenhouse gas emissions.

1.6 The thesis

The aim of this thesis was to design and synthesize an active iron based WOC in such a way that it could be immobilized onto carbon-paste electrodes[vi] with the intention of going from a homogeneous electrochemical system to a heterogeneous one. The expectations were that a heterogeneous system could increase the stability and the local concentration of the WOC on the surface of the electrode[38]. This could in turn lead to a more efficient and industrially coveted device compared to that of the homogeneous system, where the WOC instead is dissolved directly into the water. The main strategy was to use the basic catalyst skeleton of the already known WOC[39] $[Fe(bpmcn^{vii})]^{2+}$ (**6**; Figure 8) and introduce new functional groups onto the ligand structure, in order to increase the hydrophobic interaction between catalyst and electrode surface. Different synthetic approaches to the two target molecules $[Fe(bdpmcn^{viii})]^{2+}$ (**7**, Figure 8) and $[Fe(bpdcn^{ix})]^{2+}$ (**8**, Figure 8) were tested, leading up to one final iron based WOC (**8**) suitable for water oxidation on carbon paste electrodes.

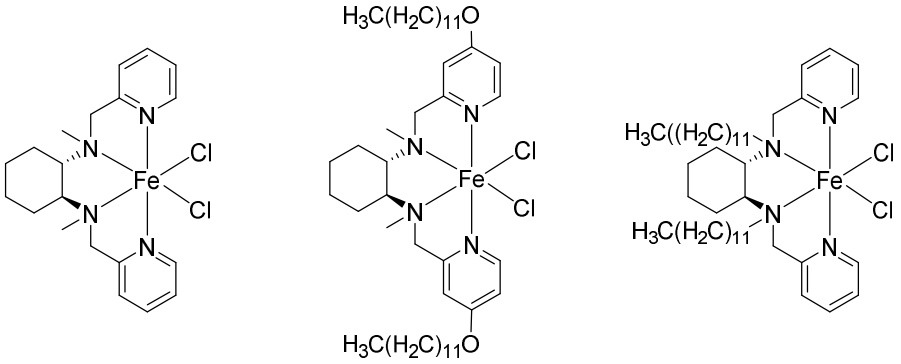

Figur 2. Benjamin M. Klepser and Bart M. Bartletts iron based WOC **6**=$Fe(bpmcn)^{2+}$ and the target molecules of this thesis **7**=$[Fe(bdpmcn)]^{2+}$ and **8**=$[Fe(bpdcn)]^{2+}$.

[vi] The carbon-paste electrode (CPE) is an electrode made from a mixture of a pasting liquid and conducting graphite powder.
[vii] bpmcn = N,N-bis(2-methylpyridyl)-N,N-dimethylcyclohexyldiamine.
[viii] bdpmcn = N,N-bis(2-methyl-4-dodecoxypyridyl)-N,N-dimethylcyclohexyldiamine.
[ix] bpdcn= N,N-bis(2-methylpyridyl)-N,N-didodecylcyclohexyldiamine.

2 Experimental

2.1 Synthesis

All chemicals used in the syntheses were obtained from Sigma Aldrich. All reactions were carried out under nitrogen atmosphere and vigorous stirring. Analytical HPLC was carried out on an Agilent Series 1100 system using either an ACE C8 (3 µm, 3.0x50 mm) column with 0.1% TFA in MilliQ H_2O / CH_3CN as mobile phase (Acidic system) or an XTerra (3.5µm 3.0x50mm) column with 10mM pH10 NH_4HCO_3 / CH_3CN as mobile phase (Basic system). Electrospray mass spectrometry (ES-MS) was performed using an Agilent 1100 Series Liquid Chromatograph/Mass Selective Detector (MSD) to obtain the pseudo molecular $[M+H]^+$ ion of the target molecules. All chromatograms were monitored between 210-305 nm. Microwave reactions were performed with a Biotage Initiator instrument using 2-5 mL or 10-20 mL Biotage Process Vials fitted with aluminum caps and septa. ^{1}H NMR spectra were recorded on a Bruker 500 or Bruker 400 instrument. All spectra were recorded using the residual solvent proton resonance.

2.1.1 Synthesis of the reference $[Fe(bpmcn)]^{2+}$

The synthesis of **6** was carried out according to reported methods in the literature[30] and the sequence is presented in Scheme 1. Thus, 508 mg (4 mmol) of 2-chloromethylpyridine hydrochloride (**6a**, Scheme 1), 284 mg (2 mmol) (1S,2S)-N,N'-dimethyl-1,2-cyclohexanediamine (**6b**, Scheme 1) and 0.55 mL (2 mmol) of Et_3N were mixed in 25 mL CH_3CN and refluxed at 85 °C for 12 h. After reaction completion, the solvent was removed by a rotatory evaporator and product **6c** was dissolved in 30 mL DCM. The organic phase was washed with 3 x 10 mL aqueous sat. K_2CO_3 solution and dried over Na_2SO_4. The solvent and remaining Et_3N was removed in vacuum at 40 °C overnight. The isolated yield of step 1 was 50%. Complexation of **6c** was carried out with anhydrous $FeCl_2$ (127 mg, 1 mmol) in CH_3CN at room temperature. Complex **6** was obtained as a precipitate after 12 h which was isolated with filtration as a yellow powder. The second reaction step yield was 69% resulting in a total yield of 34.5% over 2 steps. Attempted ^{1}H NMR measurements of **6** were performed in different deuterated solvents without success. Structural determination of **6c** was obtained by ^{1}H NMR: (500 MHz, chloroform-d) δ ppm 1.25 (m, 2 H) 1.4 (m, 2 H) 1.88 (m, 2 H) 2.20 (m, 2 H) 2.55 (br s, 3 H) 3.20 (m, 1 H) 4.5 (dd, 2 H) 7.60 (dd, 1 H) 7.95 (td, 1 H) 8.2 (td, 1 H) 8.75 (dd, 1 H), and mass of **6** by ESI-MS: *m/z* 415.27 $[M+H^+]$ (80%) 451.1 $[M+H^+]$ (20%).

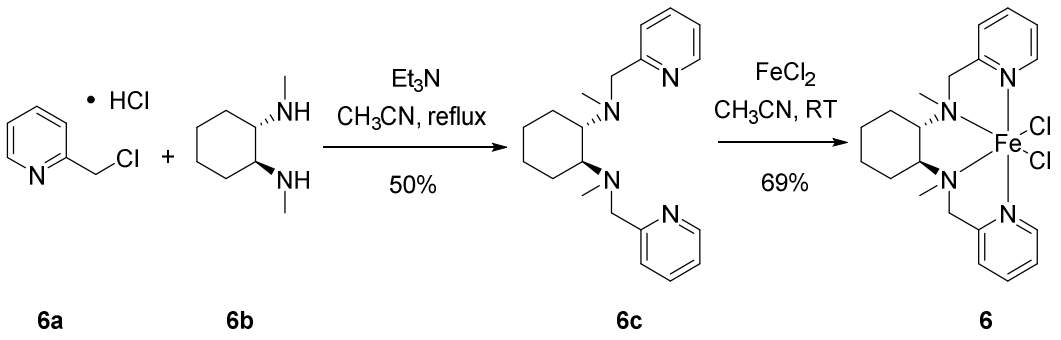

Scheme 1. Synthesis of complex **6**.

2.1.2a Attempted synthesis of $[Fe(bdpmcn)]^{2+}$

To a mixture of 0.42 g (3 mmol) 4-hydroxypyridine-2-carboxylic acid, (**7a**, Scheme 2) in EtOH (10 mL) was added conc. HCl (10 drops). By using a capped microwave-oven vial, the mixture was heated at 140 °C for 75 minutes at very high radiation program setting in a microwave oven. After cooling to RT, the mixture was filtered and the starting material **7a** was obtained as the retentate. Ethyl 4-hydroxypyridine-2-carboxylate **(7b**, Scheme 2) was isolated from the filtrate after evaporation of the solvent furnishing 201 mg (48%) product. To a solution of the product **7b** (201.0 mg, 1.2 mmol) from the previous step, in CH_3CN (20 mL) was added 1-bromododecane (0.3 mL, 1.2 mmol), KI (10 mg, 60 µmol) and K_2CO_3 (257 mg, 2 mmol). The mixture was refluxed at 85 °C for 18 h. After cooling to RT the solvent was removed in vacuum and the crude residue dissolved in DCM (20 mL). The organic phase was washed with water (3x5 mL), dried over Na_2SO_4, filtered, and the filtrate evaporated to furnish 281 mg (70%) of ethyl 4-dodecyloxypyridine-2-carboxylate (**7c**, Scheme 2) as yellow oil. ^{1}H NMR (400 MHz, chloroform-d) δ ppm 0.88 (t, 3 H) 1.1 (t, 3 H) 1.25 (br s, 16 H) 1.4 (p, 2 H) 1.75 (q, 2 H) 4.05 (q, 2 H) 4.15 (t, 2 H) 7.24 (dd, 1 H) 7.51 (ds, 1 H) 8.48 (d, 1 H). ESI-MS: *m/z* 336.25 [M+H$^+$] (100%).

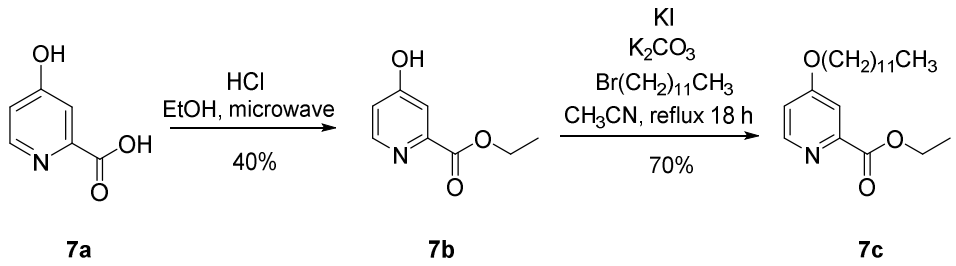

Scheme 2. First two steps in the attempted synthesis of **7**.

2.1.2b Attempted reduction of ethyl 4-dodecyloxypyridine-2-carboxylate with $NaBH_4$

To a solution of **7c** (100 mg, 0.3 mmol) in THF (20 mL) and MeOH (2 mL) was added $NaBH_4$ (20 mg, 0.6 mmol) slowly at RT. The mixture was refluxed at 66 °C for 12 h. After cooling to RT, HCl solution (1M) was added dropwise until pH 8. Water (5 mL) was added to the mixture, thereafter the MeOH and the THF was removed in vacuum and the crude residue was dissolved in DCM (30 mL). The organic phase was washed with water (3x10 mL), dried over Na_2SO_4, filtered, and the filtrate evaporated to furnish 94 mg of recovered **7c** as yellow oil. ^{1}H NMR and HPLC-MS show no trace of expected product 2-hydroxymethyl-4-dodecyloxypyridine (**7d**, Scheme 3). ^{1}H NMR (400 MHz, chloroform-d) δ ppm 0.88 (t, 3 H) 1.25 (br s, 16 H) 1.4 (p, 2 H) 1.75 (q, 2 H) 4.05 (q, 2 H) 4.15 (t, 2 H) 7.24 (dd, 1 H) 7.51 (ds, 1 H) 8.48 (d, 1 H). ESI-MS: *m/z* 336.25 [M+H$^+$] (100%).

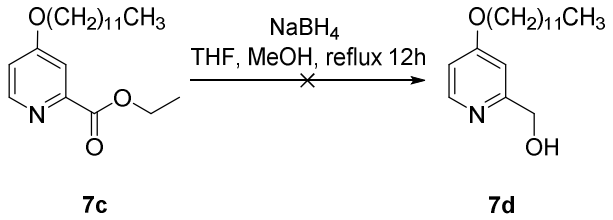

Scheme 3. Attempted reduction of **7c** with $NaBH_4$.

2.1.2c Reduction of ethyl 4-dodecyloxypyridine-2-carboxylate with $LiAlH_4$

To a solution of **7c** (100 mg, 0.3 mmol) in dry THF (20 mL) was added $LiAlH_4$ (10 mg, 0.3 mmol) slowly at 0 °C. The mixture was stirred at RT for 2 h. Thereafter a HCl solution (1M) was added dropwise until pH 8. Water (5 mL) was added to the mixture and the THF was removed in vacuum. The crude residue was dissolved in DCM (30 mL). The organic phase was washed with water (3x10 mL), dried over Na_2SO_4, filtered and the filtrate evaporated to furnish 58.6 mg (20%) of yellow oil. ^{1}H NMR showed no trace of the expected product 2-hydroxymethyl-4-dodecyloxypyridine (**7d**, Scheme 3). LC-MS was successfully performed ESI-MS: *m/z* 294.26 [M+H$^+$] (70%) 264 [M+H$^+$] (25%) 278 [M+H$^+$] (5%).

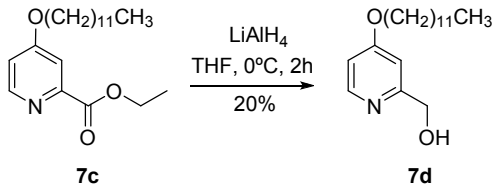

7c **7d**

Scheme 4. Reduction of **7c** with $LiAlH_4$.

2.1.2d An alternative synthesis of $[Fe(bdpmcn)]^{2+}$

To a solution of 306 mg (1 mmol) 4-dodecyloxypyridine-2-carboxylic acid (**7e**, Scheme 5) in EtOAc (25 mL) was added **6b** (71 mg, 0.5 mmol), T3P©[40] (0.6 mL, 1 mmol, 50 mol %) in EtOAc and Et_3N (0.14 mL, 1 mmol). The mixture was stirred at RT for 6 h to which thereafter was added additional T3P© (0.3 mL, 0.5 mmol). The mixture was then stirred at RT for an additional 6 h. The organic phase was washed with water (3x7 mL), dried over Na_2SO_4, filtered, and the filtrate evaporated to furnish 712 mg (99%) bcdpmcn[x] (**7f**, Scheme 5) as brown oil. ^{1}H NMR (400 MHz, chloroform-d) δ ppm 0.88 (t, 3 H) 1.25 (br s, 16 H) 1.4 (p, 2 H) 1.75 (q, 2 H) 2.85 (s, 3 H) 4.00 (q, 2 H) 4.15 (t, 2 H) 6.52 (dd, 1 H) 7.24 (ds, 1 H) 8.45 (d, 1 H). ESI-MS: *m/z* 722.56 [M+H$^+$] (60%) 361.3 [M+2H$^+$] (30%).

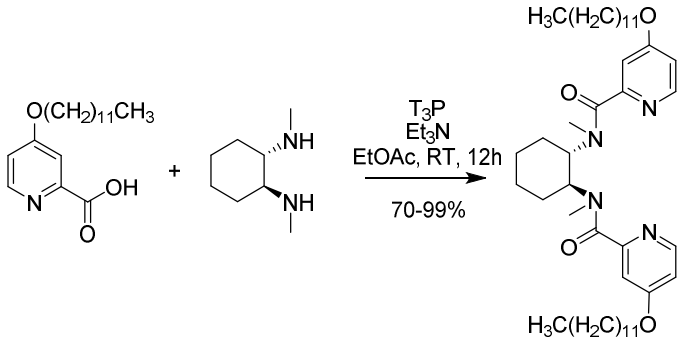

7e **6b** **7f**

Scheme 5. Synthesis of **7f**.

[x] bcdpmcn = N,N-bis(2-carboxamide-4-dodecoxypyridyl)-N,N-dimethylcyclohexyldiamine

2.1.2e Attempted first reduction of (bcdpmcn)

To a solution of **7f** (0.35 mL, 0.5 mmol) in dry THF (20 mL) was added $LiAlH_4$ (40 mg, 1 mmol) slowly at 0 °C. The mixture was stirred at 0 °C for 2 h. HCl solution (1M) was added dropwise until pH 8. Water (5 mL) was added to the mixture and the THF was removed in vacuum. The crude residue was dissolved in DCM (30 mL). The organic phase was washed with water (3x10 mL), dried over Na_2SO_4, filtered and the filtrate evaporated to furnish 0.3 mL brown oil. HPLC-ESI-MS spectrum suggested hydrolysis of amide **7f**, with the present m/z corresponding to **7h** and **7i**. ESI-MS: *m/z* 308 [M+H$^+$] (53%), 432 [M+H$^+$] (27%), 722 [M+H$^+$] (15%), 361 [M+H$^+$] 5%.

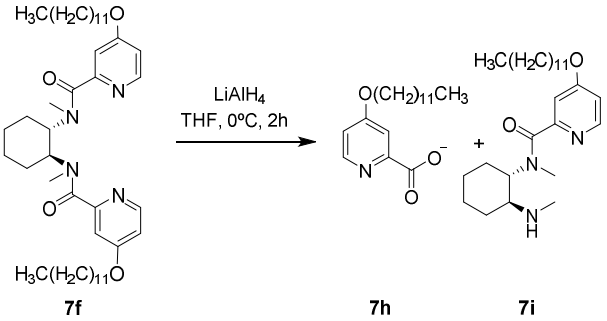

Scheme 6. Attempted reduction of **7f** to **7g** with $LiAlH_4$

2.1.2f Attempted second reduction of (bcdpmcn)

To a solution of **7f** (0.35 mL, 0.5 mmol) in MeOH (20 mL) was added $NaBH_4$ (40 mg, 1 mmol) slowly at RT. The mixture was refluxed for 12 h at 65 °C. HCl solution (2M) was added dropwise until pH 8. Water (5 mL) was added to the mixture and the MeOH was removed in vacuum. The crude residue was dissolved in DCM (30 mL). The organic phase was washed with water (3x10 mL), dried over Na_2SO_4, filtered and the filtrate evaporated to furnish 0.34 mL brown oil. HPLC-MS indicated no conversion of **7f** to desired product bdpmcn (**7g**, Scheme 6). The NMR spectrum of the isolated brown oil instead indicated the recovery of the starting material: ^{1}H NMR (400 MHz, chloroform-d) δ ppm 0.88 (t, 3 H) 1.25 (br s, 16 H) 1.4 (p, 2 H) 1.75 (q, 2 H) 2.85 (s, 3 H) 4.00 (q, 2 H) 4.15 (t, 2 H) 6.52 (dd, 1 H) 7.24 (ds, 1 H) 8.45 (d, 1 H). ESI-MS: *m/z* 722.56 [M+H$^+$] (90%) 361.3 [M+2H$^+$] (10%).

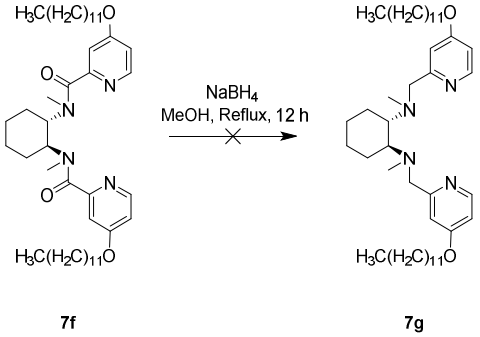

Scheme 7. Attempted reduction of **7f** to **7g** with $NaBH_4$.

2.1.3a Attempted first synthesis of $[Fe(bpdcn)]^{2+}$

To a solution of 114 mg (1 mmol) (1*S*,2*S*)-1,2-diaminocyclohexane (**8a**, Scheme 8) in CH_3CN (25 mL) was added 1-bromododecane (0.48 mL, 2 mmol) and K_2CO_3 (257 mg, 2 mmol) at RT. The mixture was refluxed for 8 h at 85 °C. After cooling to RT, K_2CO_3 was removed with filtration and the solvent in vacuum. The crude residue was dissolved in DCM (30 mL) and the organic phase was then washed with water (3x10 mL), dried over Na_2SO_4, filtered and the filtrate evaporated to furnish 0.68 mL brown oil. HPLC-ESI-MS confirmed formation of the desired product (1S,2S)-N,N'-didodecyl-1,2-cyclohexanediamine (**8b**, Scheme 8) in a mixture with the byproducts **8c** and **8d**. Purification of **8b** from the reaction mixture was attempted on silica gel and aluminum oxide columns without success. ^{1}H NMR (400 MHz, chloroform-d) δ ppm 0.88 (t, 3 H) 0.93 (m, 2 H) 1.27 (br s, 38 H) 1.45 (p, 2 H) 1.68 (m, 2 H) 2.09 (m, 2 H) 2.42 (m, 1 H) 2.75 (m, 1 H). ESI-MS: *m/z* 618 [M+H$^+$] 452 [M+H$^+$] 283 [M+H$^+$].

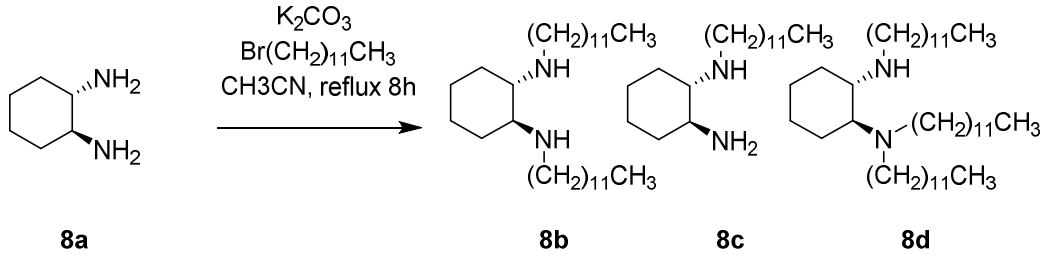

Scheme 8. Alkylation of **8a**.

2.1.3b Attempted second synthesis of $[Fe(bpdcn)]^{2+}$

To a solution of **8a** (114 mg, 1 mmol) in DCE (25 mL) was added 257 mL (2 mmol) dodecyl aldehyde (**8e**, Scheme 9) and $NaBH(AcO)_3$ (848 mg, 4 mmol) at RT. The mixture was stirred at RT for 24 h. The organic phase was washed with water (3x7 mL), dried over Na_2SO_4, filtered, and the filtrate evaporated to furnish 0.7 mL brown oil. HPLC-ESI-MS indicated a product mixture of **8b**, **8c** and **8d**. Isolation of **8b** from the product mixture was attempted without success. ^{1}H NMR (400 MHz, chloroform-d) δ ppm 0.88 (t, 3 H) 0.93 (m, 2 H) 1.27 (br s, 38 H) 1.45 (p, 2 H) 1.68 (m, 2 H) 2.09 (m, 2 H) 2.42 (m, 1 H) 2.75 (m, 1 H). ESI-MS: *m/z* 618 [M+H$^+$] 452 [M+H$^+$] 283 [M+H$^+$].

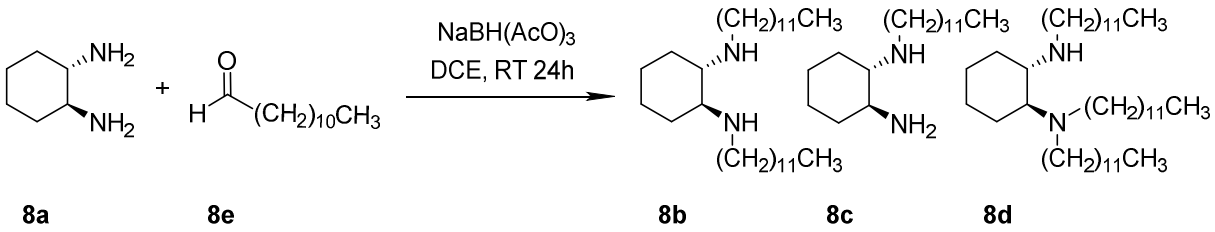

Scheme 9. Reductive amination of **8a**.

2.1.3c Attempted third synthesis of $[Fe(bpdcn)]^{2+}$

To a solution of **8a** (114 mg, 1 mmol) in MeOH (25 mL) was added **8e** (257 mL, 2 mmol) at RT. The mixture was stirred at RT for 2 h. The reaction was monitored by HPLC and ^{1}H NMR. After full conversion of the starting materials to (1*S*,2*S*)-*N*,*N*-didodecylidene-1,2-cyclohexanediamine (**8f**, Scheme 10), $NaBH_4$ (78 mg, 2 mmol) was slowly added to the reaction mixture at RT. The mixture was heated to 50 °C for 23 h. HCl solution (1M) was added dropwise until pH 8. Water (5 mL) was added to the mixture and the MeOH was removed in vacuum. The crude residue was dissolved in DCM (30 mL). The organic phase was washed with water (3x10 mL), dried over Na_2SO_4, filtered and the filtrate evaporated to furnish 0.59 mL brown oil. HPLC-MS indicated a product mixture of **8b**, **8c** and **8d**. Isolation of **8b** was attempted without success. ^{1}H NMR (400 MHz, chloroform-d) δ ppm 0.88 (t, 3 H) 0.93 (m, 2 H) 1.27 (br s, 38 H) 1.45 (p, 2 H) 1.68 (m, 2 H) 2.09 (m, 2 H) 2.42 (m, 1 H) 2.75 (m, 1 H). ESI-MS: *m/z* 618 [M+H$^+$] 452 [M+H$^+$] 283 [M+H$^+$].

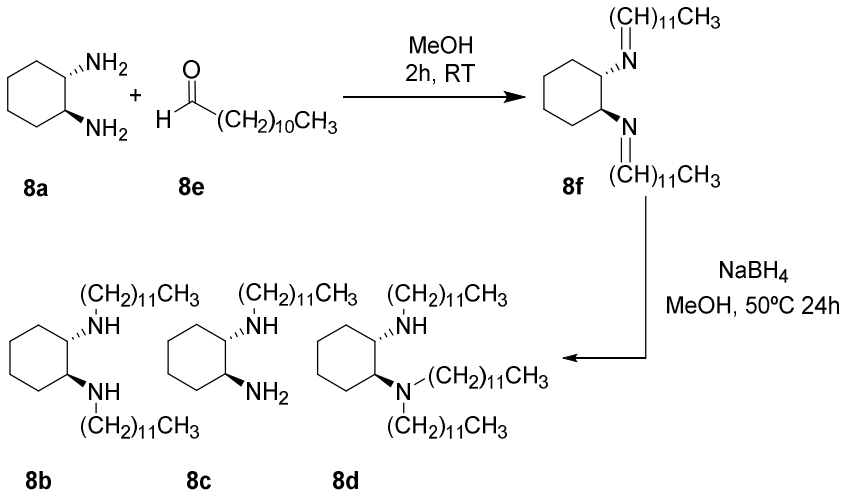

Scheme 10. Imine formation of **8a** and **8e** followed by reduction with $NaBH_4$.

2.1.3d Synthesis of $[Fe(bpdcn)]^{2+}$

To a solution of **8a** (114 mg, 1 mmol) in EtOH (25 mL) was added 0.2 mL (2 mmol) 2-pyridinecarboxaldehyde (**8g**, Scheme 11) at RT. The mixture was refluxed for 2 h at 79 °C. The solvent was thereafter reduced in volume to 7 mL in vacuum and the crude mixture was cooled in a freezer at -18 °C for 12 h. The grown yellow crystals in the mixture were filtered and washed with cold (0 °C) EtOH to furnish 277 mg (95%) of (S,S)-bis-2-pyridinylmethylene-1,2-cyclohexanediamine (**8h,** Scheme 11). **8h** (277 mg, 0.95 mmol) was thereafter dissolved in 20 mL MeOH. $NaBH_4$ (80 mg, 2 mmol) was added and the mixture was stirred at RT for 2 h. The mixture was thereafter refluxed at 66 °C for 2 h. HCl solution (2M) was added dropwise to the mixture until pH 8. Water (5 mL) was added to the mixture and the MeOH was removed in vacuum. The crude residue was dissolved in DCM (30 mL). The organic phase was washed with water (3x10 mL), dried over Na_2SO_4, filtered and the filtrate evaporated to furnish 253 mg (90%) (1*S*,2S)-*N*,*N*-bis(2-pyridinylmethyl)-1,2-cyclohexane-diamine (**8i**, Scheme 11) as amber oil.

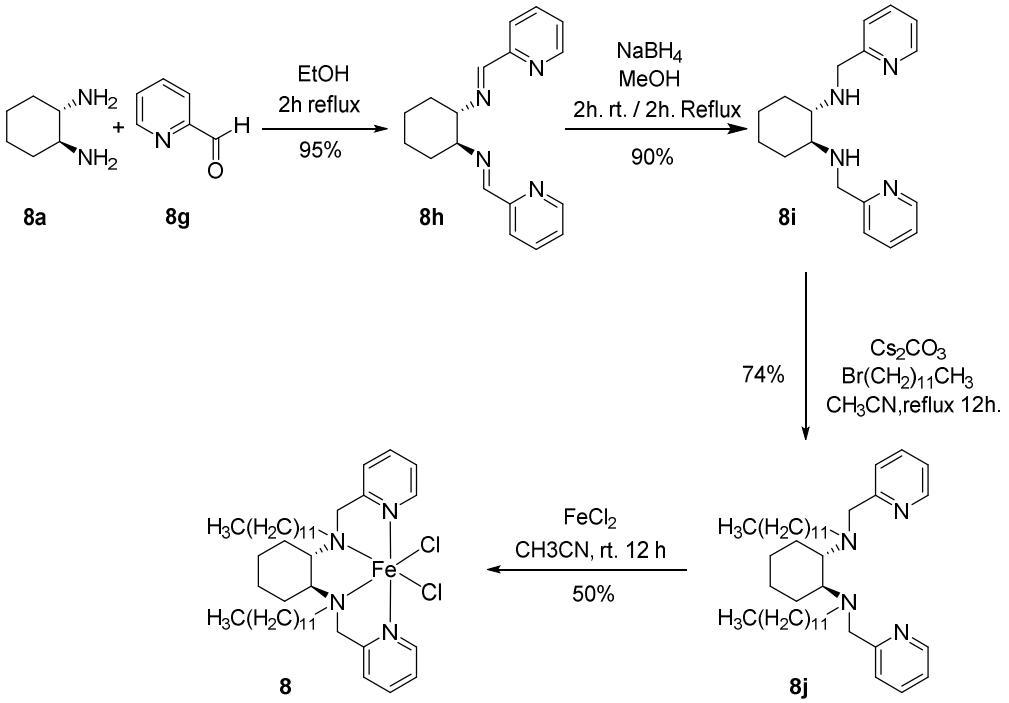

Scheme 11. Full synthesis of **8**.

8i (253 mg, 0.85 mmol) was thereafter mixed with Cs_2CO_3 (651 mg, 2 mmol) and bromododecane (0.5 mL, 2 mmol) in CH_3CN at RT. The mixture was refluxed at 85 °C for 12 h. After cooling the mixture to RT, the Cs_2CO_3 was removed with filtration and the solvent was removed in vacuum. The crude residue was dissolved in DCM (25 mL) and the organic phase was washed with water (3x7 mL), dried over Na_2SO_4, filtered, and the filtrate evaporated. The product mixture was purified on a sephadex© column with $CHCl_3$ as eluent. The pure fractions were combined furnishing 400.6 mg (74%) of the ligand bpdmcn (**8j**, Scheme 11). ^{1}H NMR (400 MHz, chloroform-d) δ ppm 0.88 (t, 3 H) 1.23 (br s, 16 H) 1.4 (m, 2 H) 1.75 (m, 1 H) 2.1 (m, 1 H) 2.5 (m, 2 H) 2.42 (m, 1 H) 2.75 (m, 1 H) 3.6 (d, 1 H) 3.8 (d 1H) 7.05 (td, 1 H) 7.45 (td, 1 H) 7.6 (dd, 1 H) 8.45 (dd, 1 H). ESI-MS: *m/z* 317 $[M+2H^+]$ (60%) 634 $[M+H^+]$ (40%). To **8j** (398 mg, 0.62 mmol) in CH_3CN (15 mL) was added anhydrous $FeCl_2$ (126 mg, 1 mmol). The mixture was then stirred at RT for 12 h. The mixture was filtered and the retentate washed with CH_3CN furnishing 240 mg (50%) title product **8.**

2.2 Functionalization of the electrode

2.2.1 Preparation of the carbon paste electrode

50 g paraffin wax (ASTM D 127) was melted at 80 °C in a 200 mL beaker and was thereafter mixed with 50 g carbon black for 10 minutes. The carbon paste was then let to cool down to room temperature and harden for one hour. The paste was then grounded with the help of a mortar to 1 mm ⌀ particles and 1 g was placed in a hydraulic IR pellet press. With an applied force of 10 ton, the particles were compressed for 10 minutes. The formed carbon paste pellet was thereafter removed from the press and pierced with a paperclip halfway through.

2.2.2 Immobilization of $[Fe(bpdcn)]^{2+}$ onto carbon paste electrode

380 mg (0.5 mmol) $[Fe(bpdcn)]^{2+}$ was dissolved in 1 mL $CHCl_3$ and applied onto the carbon paste electrode surface with a 1 mL syringe by drop casting. Deposition was carried out in batches and the solvent was allowed to evaporate from the surface of the electrode before more complex solution was added. After completion of the deposition, the surface of the electrode had turned from gray to brown color.

2.3 Electrochemical measurements

Bulk electrolysis and cyclic voltammetric (CV) measurements were carried out with an Autolab potentiostat with a GPES electrochemical interface (Eco Chemie) with pyrolytic graphite electrode (either basal or edge plane) as working electrodes, and a Pt wire as auxiliary electrode, and measured versus SCE reference electrode. The scan rate was set to 0.1 V/s. All reported potentials have been converted to their corresponding value versus Ag/AgCl, using an internal reference $[Ru(bpy)_3]^{2+}$ ($E_{1/2}(Ru^{III/II})$ = 1.26 V versus NHE). The phosphate buffer solution was bought premixed from Sigma Aldrich and acetonitrile buffer was prepared to 0.1 M with tetrabutylammonium hexafluorophosphate.

2.3.1 Cyclic voltammetry of $[Fe(bpmcn)]^{2+}$ in different buffer solutions

CV of $[Fe(bpmcn)]^{2+}$ was first performed in a mixture of 2 mL 0.1 M phosphate buffer (pH 7) mixed with 2 mL 0.1 M acetonitrile buffer solution and recorded from 0 V to +1.2 V. The CV was then evaluated against the CV record obtained in blank phosphate-acetonitrile buffer mixture. Thereafter CV of $[Fe(bpmcn)]^{2+}$ in 2 mL water (pH 7) and 2 mL 0.1 M acetonitrile buffer was performed and recorded from 0 V to +1.2 V. The obtained CV was evaluated against the recorded blank deionized water-acetonitrile buffer mixture.

2.3.2 Cyclic voltammetry of $[Fe(bpdcn)]^{2+}$ doped CPE before and after electrolysis

CV of $[Fe(bpdcn)]^{2+}$ doped CPE was performed in a mixture of 2 mL 0.1 M acetonitrile buffer solution mixed with 2 mL deionized water and recorded from 0 V to +1.2 V. The CV was then evaluated against the CV record obtained after performed electrolysis with $[Fe(bpdcn)]^{2+}$ doped CPE and blank CPE under same conditions before and after electrolysis.

2.3.3 Electrolysis of water with $[Fe(bpdcn)]^{2+}$ doped CPE

Electrolysis of water with $[Fe(bpdcn)]^{2+}$ doped CPE (anode) and Pt wire net electrode (cathode) was performed in 10 mL deionized water under continuous stirring to remove bubbles from surface of the electrode. A potential of 1.5 V was applied for 2500 s. The performance of the electrode was then evaluated against the recorded blank CPE under the same conditions.

3 Results and Discussion

3.1 Synthetic and analytical results

3.1.1 Characterization of the reference $[Fe(bpmcn)]^{2+}$ (6)

The structural determination of **6**, with the use of NMR, was attempted in various solvents[xi] without further success. After the complexation of **6c** with $FeCl_2$, a total loss of the signals associated with the ligand was observed. This phenomenon was proposed to come from the paramagnetic behavior of iron(II)[41]. The two unpaired d-electrons of the iron center atom, together with the absence of strong field ligands in **6** suggest a possible paramagnetic species. In typical paramagnetic materials, each individual electron spin is unaffected by its neighbors. The spins of a paramagnetic material can easily be aligned by an applied magnetic field. However the alignment is weak, and upon removal of the magnetic fields the system relaxes back to a random distribution of magnetic moments. This often causes broadening of signals, partial or total loss of the spectrum as in the case of **6**. Mass spectrometry could be used to determine the molecular weight of **6** which corresponded to theoretical value of 451.1 g/mol.

3.1.2 Synthesis of 7 and the reduction of ethyl 4-dodecyloxypyridine-2-carboxylate (7c)

During the designing stages of **7**, the general idea was to introduce hydrophobic functional groups to the ligand structure of **6** in a way that would improve the adsorption of the complex onto the surface of the electrode. The placement of the functional groups was deliberately and carefully thought through, so that they would not interfere with the accessibility of water during coordination. It was hypothesized that positioning of the alkyl chain in position 5 or 6 of the pyridine could obstruct water from approaching and coordinate with the active center. Position 3 was considered but due to the synthetic simplicity and commercial availability of the starting compound **7a,** the complex **7** was chosen as a first candidate.

When working towards **7**, the synthetic pathway of **6** was utilized. The planed step after obtaining **7d** was to use thionyl chloride, to transform the pyridine alcohol into the corresponding chloromethyl pyridine, followed by a substitution reaction with **6b**. The reduction of **7c** was initially attempted with $NaBH_4$ (reaction 2.1.2b) as it according to literature[42] is a suitable reducing agent for similar reactions. However, neither HPLC-ESI-MS nor ^{1}H NMR[xii] indicated any conversion of the ester to the expected alcohol. Posterior disclosure suggests that the $NaBH_4$ used in 2.1.2b had been stored inappropriately which is why it is suggested to repeat this experiment with active $NaBH_4$.

During the project, $NaBH_4$ was assumed to be too weak of a reducing agent to reduce **7c** to **7d**. This is the reason to why instead the more potent reducing agent $LiAlH_4$ was utilized. In experiment 2.1.2c the product was obtained as insoluble paste, reminiscent of tar after workup. ^{1}H NMR of the product **7d** was performed but did not supply any helpful information[xiii]. The mass spectrometry indicated formation of product together with further fragmentation and reduction of the alcohol. It is likely that the lithium hydroxide and aluminum hydroxide salts had formed during the reduction and that the attempted workup method was not apt for **7d**. Instead, a basic workup according to the method

[xi] See Appendices Solvents and solvent systems Table 17.
[xii] See Appendices ^{1}H NMR spectra Table 3 and HPLC chromatograms and MS spectra Table 9.
[xiii] See Appendices ^{1}H NMR spectra Table 4 and HPLC chromatograms and MS spectra Table 10.

by Fieser, could be a more suitable for this reaction. Due to the timeframe of the project, the first planed synthesis path was here put on hold.

3.1.3 The second synthesis path for 7 and the reduction of (bcdpmcn) (7f)

After the attempted reduction of **7c**, an alternative pathway was perused in the synthesis of **7** (synthesis 2.1.2d). By utilizing the coupling reagent T3P©, **7f** was successfully obtained in a yield of 99%. The subsequent step of the synthesis would be to reduce the diamide and form **7g**. As amides often require stronger reducing agents, $LiAlH_4$ was used first. However, during analysis of the product, it would appear that $LiAlH_4$ was too strong as a reducing agent, as it under the tested conditions split **7f**, yielding primary amine and carboxylate fragments[xiv].

Based on this knowledge, the reduction **7f** with the less active $NaBH_4$ was attempted. $NaBH_4$ is a schoolbook example of a reducing agent that seldom reduces amides which was observed during the analysis of the non-transformed starting material[xv]. Other options were thought of but due to the lack of time, the synthesis of **7** was put on a hold.

3.1.4 Analysis and purification of (1S,2S)-N,N'-didodecyl-1,2-cyclohexanediamine (8b)

Simultaneously, while developing a synthesis of **7**, the secondary WOC candidate **8** was designed, starting with the attempted reaction 2.1.3a. The idea of **8** was to, in a similar manner to the synthesis of **6**, react an alkylated 1,2-diaminocyclohexane with **6a** to form the complete ligand structure in a two-step synthesis. The electrode-anchoring groups would now be the dodecyl substituents, attached directly to the nitrogen atoms of the diamine. The reason to this was to bypass the synthetic obstacle that was encountered earlier with **7c** and also to further direct the rear of the complex more towards the electrode surface during immobilization. After performing the reaction 2.1.3a, a ^{1}H NMR spectrum of the crude showed the formation of the desired product. However further analysis of the crude with HPLC-MS revealed a mixture of three products **8b**, **8c**, and **8d**[xvi]. It appeared that the peaks of the three products overlap with those of the product, which makes it hard to analyze the mixture by ^{1}H NMR. In an attempt to separate the three products, different TLC systems of eluents[xvii] were tested and flash chromatography was performed without successful separation. It is plausible that the long carbon chains on the amines could cause the products to co-eluate, together with the influence of the nitrogens causing tailing on the column. In the attempts of avoiding formation of the byproducts, the reaction sequences 2.1.3b and 2.1.3c were tested. By first forming the corresponding imine followed by reduction, it was hoped for a more desired product-yielding reaction. Mass spectrometry revealed that in both 2.1.3b and 2.1.3c, the two undesired byproducts had formed[xviii] making it hard isolate **8b**. With this knowledge, a new pathway was attempted (reaction 2.1.3d) which made it possible to isolate the final complex **8**.

[xiv] See Appendices HPLC chromatograms and MS spectra Table 11.
[xv] See Appendices ^{1}H NMR spectra, Table 6 and HPLC chromatograms and MS spectra Table 12.
[xvi] See Appendices ^{1}H NMR spectra, Table 7 and HPLC chromatograms and MS spectra Table 13.
[xvii] See Appendices Solvents and solvent systems Table 17.
[xviii] See Appendices HPLC chromatograms and MS spectra, Table 14 and MS Table 15.

3.1.5 Successful synthetic route for $[Fe(bpdcn)]^{2+}$ (8)

The previously encountered problems with the overalkylation of the diamine in 2.1.3a-c were bypassed in the pathway described in 2.1.3d. As a result of the difficult workup procedures that followed in 2.1.3a-c, the idea had changed to add the dodecyl chains lastly as a precaution to prevent mono- and tri-dodecylation of the diamine. The outline was similar to that of reaction 2.1.3c, but with crystallization as an intermediate workup procedure, the amount of byproducts could be kept low. As of 2.1.3c, the aliphatic chains of the dodecyl groups made it hard to grow crystals, which is why this method was not utilized in previous reactions. The previously gained experience of how dodecylated amines behave on silica gel column had turned the attention to Sephadex. The size exclusion gel would show to fit the project and was therefore used for purification of both ligand **7d,** and complex **8**. **8** would show to have the same paramagnetic properties as **6** with the same iron(II) core, which limited the analytical options of the complex. For this reason, the presented ^{1}H NMR data is of the ligand **7d** before the complexation. HPLC-ESI-MS measurements of ligand **7d** were successfully performed and agreed with theory[xix] with a m/z value of 634. As for the electrochemical measurements, the crude of the product mixture from 2.1.3d was used. It was later on, after completion of the project, confirmed that the mass of the crude corresponded to that of complex **8.** However traces of impurities were also found and it is therefore suggested to purify the crude mixture and redo electrochemical measurements as an extra precaution.

[xix] See Appendices ^{1}H NMR spectra, Table 8 and HPLC chromatograms and MS spectra Table 16.

3.2 Electrochemistry

3.2.1 Effects of phosphate buffer solution on [Fe(bpmcn)]2+ (6)

During the potentiodynamic electrochemical measurements of the reference complex **6**, an unexpected observation was made. While recording a cyclic voltammogram of **6** in a 50:50 mixture of phosphate buffer (pH 7) and acetonitrile buffer, no reversible peak related to oxidation could be observed. However, when the system was changed to a 50:50 mixture of water (pH 7) and acetonitrile buffer solution, a clear reversible peak at 0.5 V would appear. A comparison with blank buffer solution was then performed, in which no reversible peak was observed. This would indicate that the buffer solution alone can't be beholden to the catalytic oxidation seen at 0.4 V, but rather that the presence of **6** is the source of this phenomenon (Figure 9; **B**).

The evanescent peak of oxidation in the phosphate buffer solution (Figure 9; **A**) is believed to come from the rapid formation of iron phosphate during measurements. As a remark, according to literature[38], ligand **6c** is not active towards water oxidation. It is therefore suggested that complex **6** could either bond covalently with phosphate and prohibit the access of water to the reactive center or that a ligand exchange reaction take place during the measurements causing $Fe_3(PO_4)_2$ to precipitate out of the solution relinquishing the inactive ligand. Observations of the testing vials show that a brown precipitate start to form a few hours after the measurements. It would be of great interest to analyze the brown precipitate to clarify if it is a salt or a complex as this was postponed in the project.

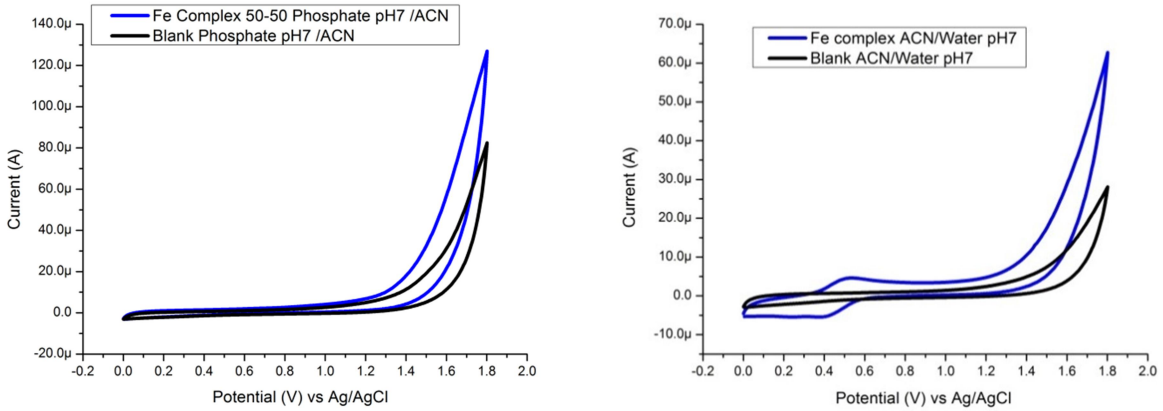

A **B**

Figure 3. A represent a CV of $[Fe(bpmcn)]^{2+}$ in 50:50 phosphate-acetonitrile buffer solution, vs blank buffer solution mixture of same composition**. B** represent a CV of $[Fe(bpmcn)]^{2+}$ in 50:50 water (pH 7)-acetonitrile buffer solution, vs blank buffer solution mixture of same composition.

3.2.2 Electrolysis of water with $[Fe(bpdcn)]^{2+}$ doped CPE

When performing electrolysis with the **8**-doped carbon paste electrode in water (Figure 10), an increase in catalytic current was observed compared to that of the blank CPE. An applied potential of 1.5 V was used and the measurements went on for 2500 s. The recorded current of the electrode was seemingly high at the start of the measurements at around 73 µA for the doped CPE and 15 µA for the blank. This had to do with the discharge of a build-in capacitor of the potentiostat and should be disregarded.

A continued decrease in current was observed throughout the electrolysis. This phenomenon was suggested to come from decomposition or desorption of the catalyst from the electrode during measurements. The evolution of oxygen on the surface of the electrode was believed to causes the applied layer of catalyst to slowly abrase over time. The desorption of **8** from the surface of the electrode would cause it to float to the top of the testing vial, as the density of **8** is much lower than that of water, making it impossible for recordation of the complex back to the electrode surface. An observation that would strengthen this theory was that at the end of measurements a thin yellow lamina would appear at the surface of the testing vial. After 2500 s of measurements the catalytic current had dropped to 10 µA which was 23% of initial current.

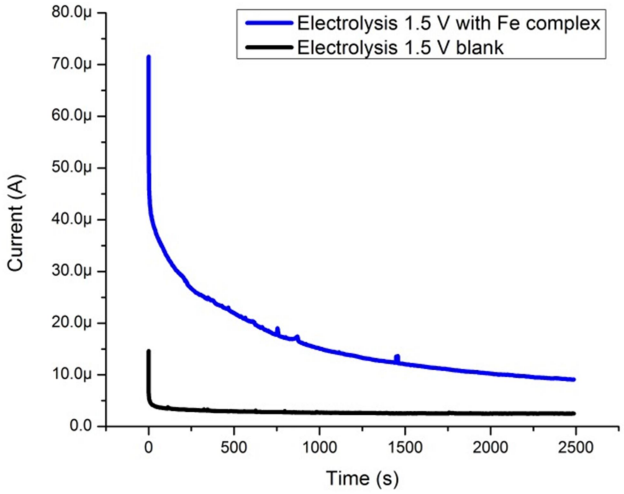

Figure 4. Electrolysis of water with $[Fe(bpdcn)]^{2+}$ doped electrode (blue) compared to electrolysis of water with a blank CPE (black). An applied potential of 1.5 V vs Ag/AgCl was used for 2500 s.

The initial catalytic current was obtained from CV measurements (Figure 11) of the doped electrode prior to the electrolysis. During electrolysis, a potential of 1.5V was applied to the electrode which according to Figure 11 corresponded to a catalytic current of 63 µA in the CV.

From the CV measurements, it would also show that the reversible oxidation peak of **8** remained present after electrolysis. This indicated that the electrode still had active **8** immobilized onto its surface and that oxidation would still occur at 0.5 V.

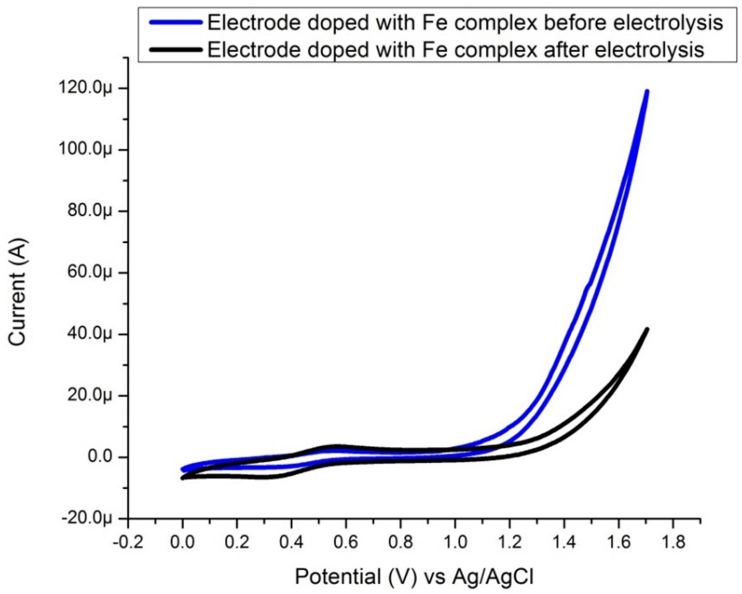

Figure 11. CV of the $[Fe(bpdcn)]^{2+}$ doped electrode before and after electrolysis of water.

At higher overpotential the difference in performance is clearer as the difference in catalytic current increases with increased applied voltage. Another observation that indicates a loss of activity is the dislocation of the increment of the slopes. Before electrolysis the catalytic current starts to increase at around 1 V but after performed measurements, instead an applied voltage of 1.2 V is needed before a visible increase of current start to show. The fact is that they both start at the same potential but the increment is so small looks like a plateau.

3.2.3 Stability testing of the carbon paste electrode

It was of great interest to see if a possible degradation of the electrode could be the cause of the decreasing performance of the device during electrolysis. The conductivity of the CPE is related to how ragged the surface is in a negative manner. Tests to see if the decreasing performance of the device were related to the decomposition of the electrode were therefore carried out. If the matrix of the electrode would be distorted from the oxygen evolution, it could cause small pieces of the electrode to leave along with immobilized complex, resulting in a drop of performance.

A CV of a blank electrode was recorded from 0 to 1.7 V before the electrolysis of water. After performed electrolysis, another CV of the electrode was recorded (Figure 12) under prior conditions. The extra 0.2 V were added as a safety precaution to see if the electrode could withstand higher potentials than the one used during electrolysis. At 1.5 V, a difference in current of about 1 µA was recorded. When the potential was increased to 1.8 V the difference in current was larger with 29 µA before and 22 µA after electrolysis. Accordingly, it is possible that oxidation or decomposition of the electrode could have occurred during electrolysis. These are factors which could have contributed to the decreasing performance of the device.

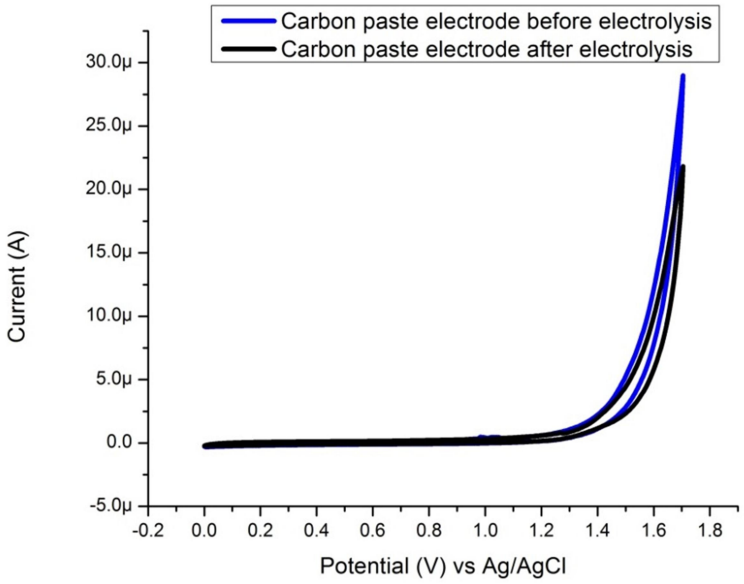

Figure 12. Stability testing of the carbon paste electrode before and after electrolysis of water.

3.3 Suggestions for future studies

For the future studies and the continuation of this project a few suggestions from the author are to be presented.

To verify the correct structure of **6** from synthesis 2.1.1, it is suggested to use an alternative method of qualitative analysis called electron spin resonance (ESR) spectroscopy. The method is mostly used for analysis of materials with unpaired electrons as it compared to NMR excites the spins of the electrons in the nuclei of the atoms instead of the valence electrons[43].

It would be of much interest to complete the syntheses of complex **7** and compare its performance to that of **8**. If a continuation on the approach to reduce the ester from reaction 2.1.2a is favored, $NaBH_4$ would be preferred to use as a reductant over $LiAlH_4$ as it is less likely that the alcohol will undergo further reduction with $NaBH_4$. If however $LiAlH_4$ is used, a basic workup method to dissolve the formed Lithium hydroxide – Aluminum hydroxide cake, which entraps the product, can be utilized. A second option would be to use **7f** and attempt a reduction. In this case $NaBH_4$ is not suggested as it is too weak, but instead $LiAlH_4$ could be utilized. A proposal is to attempt reaction 2.1.2e but to lower the reaction temperature and decrease the amount of reductant.

It would also, for future studies, be worthwhile to investigate how the orientation of the long carbon chain substituents influences on the overall performance of the WOC. For the full study, the alkylation of the pyridine rings should take place in every different position and be compared to find an optimal case.

For the structural determination of **8**, characterization with ESR is suggested, in order to obtain the correct geometry of the complex. If possible, crystallization followed by x-ray spectroscopy could be an option but the long alkyl chains could cause complications during nucleation and propagation. Chemical analysis and MS are possible alternatives for methods of analysis.

Oxygen evolution measurements for further clarification that complex **8** work as a water oxidation catalyst should be performed as a next step of the analysis.

The evanescent oxidation peak of the CV in phosphate buffer solution is an interesting phenomenon and should be further investigated. Increasing the concentration of **6** could lead to clearer precipitation of iron phosphate which might be a cause to why the reversible oxidation peak is missing. Analyzing the precipitate with x-ray microscopy is an option to see if it consists of a homogeneous crystal matrix or a mixture of different components. Electrolysis measurements of **6** dissolved in water have to be performed to be able to compare the results of the homogeneous system to that of the heterogeneous. Oxygen evolution measurements of **6** should then also be compared with those of **8**.

It would be further worthwhile to attempt in improving the stability of the carbon paste electrode by altering the composition and the applied pressure during construction. Another option would be to change the electrode to a carbon nanotube based one, which could improve the performance of the complete system[44]. Although not brought up in this project, mechanistic studies of the complex could help in the understanding of how the complex acts as a catalyst and is therefore a topic of interest to be pursued.

4 Conclusion

The aim of this thesis was to synthesize an iron based water oxidation catalyst and to immobilize it onto a carbon paste electrode. As the application of the synthesized iron(II) centered complex **8** on CPE caused an increase in catalytic current during the electrolysis, it is fair to say that these results look promising. Before stating that the complex acts as a WOC, oxygen evolution testing have to be performed with the catalyst. For the structural determination of the paramagnetic complex **8**, ESR is suggested to be used instead of NMR which is unable to record signals from molecules containing paramagnetic properties. The electrochemical measurements of reference compound **6** provided greater understanding of iron(II) complexes sensitivity towards phosphate. In order to be able to make a comparison of performance between the two different systems of devices, electrolysis of **6,** dissolved in water, still has to be made. A continuous decrease in performance was recorded throughout the entire timespan of the electrolysis. This is suggested to come from desorption of complex to the water, the decomposition of the catalyst into $Fe_3(PO_4)_2$ and the degradation of the electrode during electrolysis.

Acknowledgements

I would like to give thanks to the following individuals for their contribution to this work:

My supervisors: Prof. Licheng Sun and PhD student Quentin Daniel for allowing me to work on this project and being my mentors during this time. I valued your input, ideas and encouragement greatly.

All the group members of the Sun group: Lei Wang, Fusheng Li, Ke Fan, Ram Ambre, Lele Duan, Bo Xu, Ming Cheng and Yong Hua for all the help you provided me with both experimentally but also from a theoretical aspect.

Fredrik Schaufelberger, Brian Timmer, Anna Laurell, Robin Hertzberg, Laure Theveau, Björn Blomkvist, Johan Franzén, Ramesh Naidu, Peter Dinér and Lei Hu for fruitful discussions and pointers.

All the employees at Organic Chemistry for the friendly atmosphere and a joyful time spent together.

Appendices

^{1}H NMR Spectra

Table 1. ^{1}H NMR of **6c** in $CDCl_3$ (synthesis 2.1.1)

^{1}H NMR of 2.1.1 bpmcn (ligand 6c)	
Chemical Formula: $C_{20}H_{28}N_4$	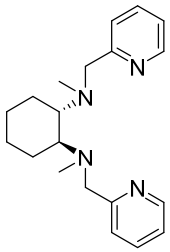
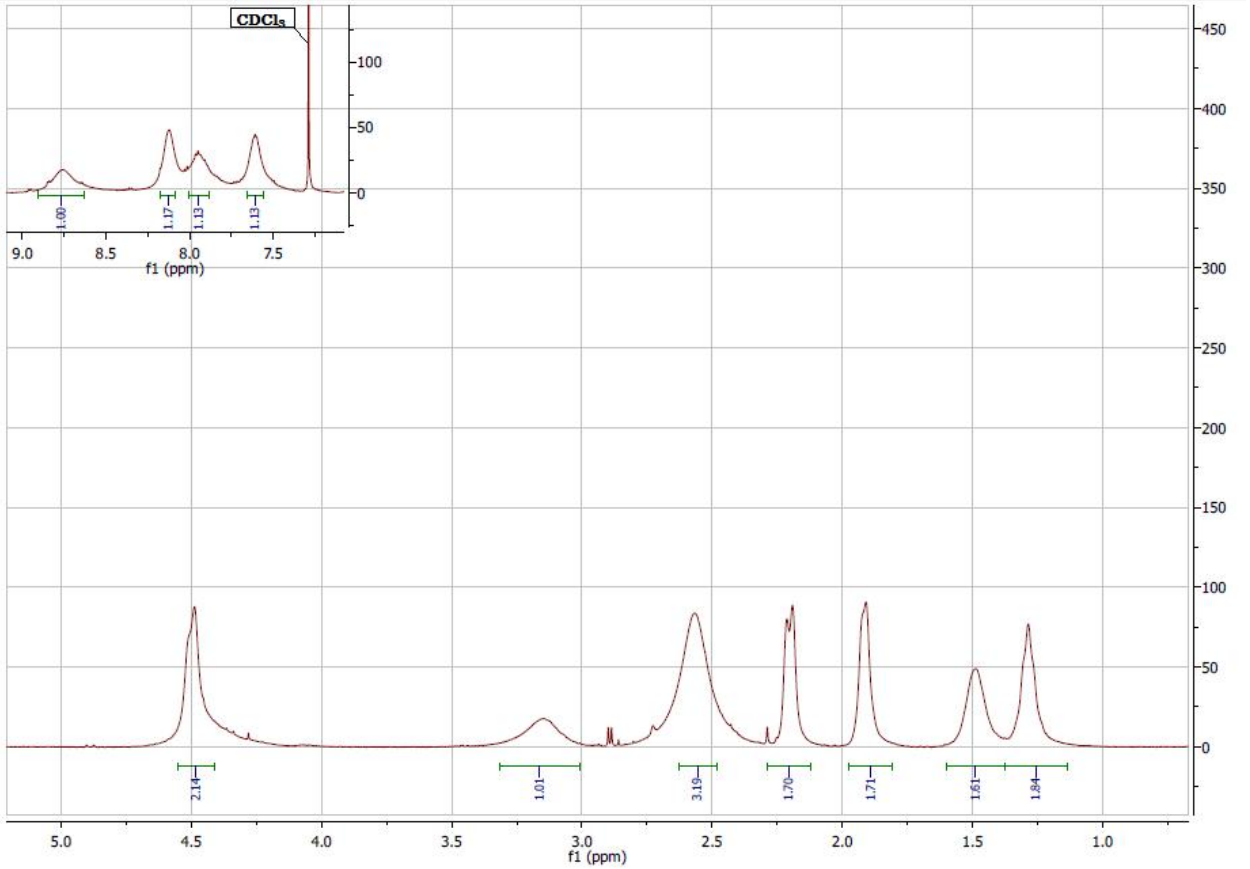	
^{1}H NMR (500 MHz, CHLOROFORM-D) δ ppm 1.25 (m, 2 H) 1.4 (m, 2 H) 1.88 (m, 2 H) 2.20 (m, 2 H) 2.55 (br s, 3 H) 3.20 (m, 1 H) 4.5 (dd, 2 H) 7.60 (dd, 1 H) 7.95 (td, 1 H) 8.2 (td, 1 H) 8.75 (dd, 1 H).	

Table 2. ^{1}H NMR of **6** in DMSO-d_6 with a few added drops of $CDCl_3$ to further improve solubility (synthesis 2.1.1).

^{1}H NMR of 2.1.1 $[Fe(bpmcn)]^{2+}$ (complex 6)	
Chemical Formula: $C_{20}H_{28}Cl_2FeN_4$	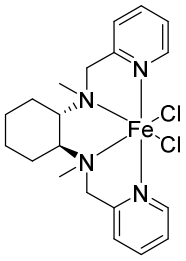
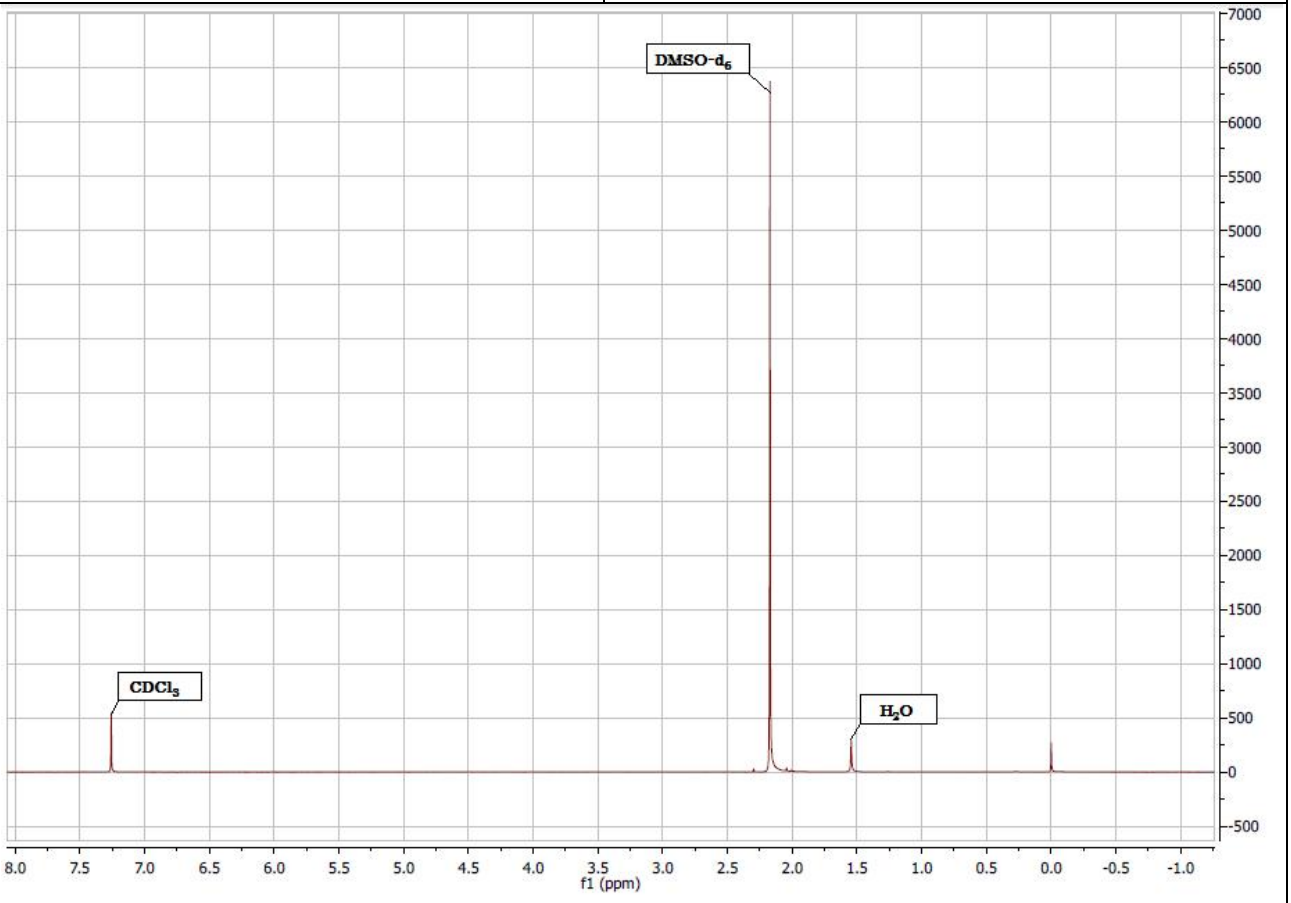	
^{1}H NMR (400 MHz, DMSO-d_6 CHLOROFORM-D) δ ppm - .	

Table 3. ^{1}H NMR of **7c** after mixing with $NaBH_4$ (synthesis 2.1.2b).

^{1}H NMR of the attempted reduction of ethyl 4-dodecyloxypyridine-2-carboxylate with $NaBH_4$	
Chemical Formula: $C_{20}H_{28}Cl_2FeN_4$	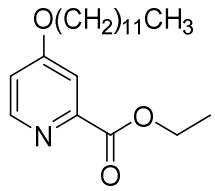

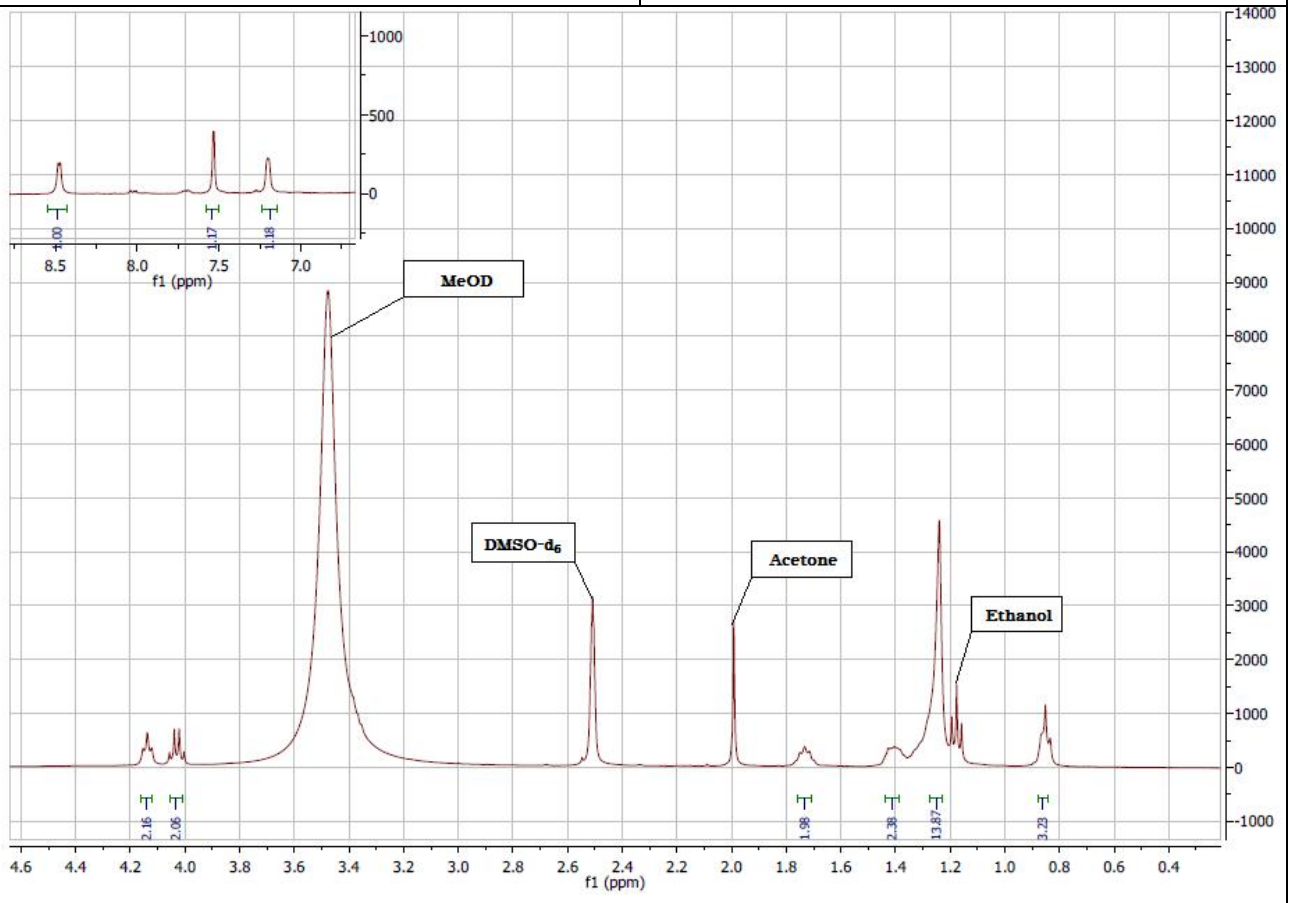

^{1}H NMR (400 MHz, chloroform-d) δ ppm 0.88 (t, 3 H) 1.25 (br s, 14 H) 1.4 (p, 2 H) 1.75 (q, 2 H) 4.05 (q, 2 H) 4.15 (t, 2 H) 7.24 (dd, 1 H) 7.51 (s, 1 H) 8.48 (d, 1 H).

(The NMR tube was washed with ethanol and acetone before measurements had started and was unfortunately not given enough time for solvent to evaporate).

Table 4. ^{1}H NMR of **7d** after attempted acidic workup (synthesis 2.1.2c).

^{1}H NMR of the reduction of ethyl 4-dodecyloxypyridine-2-carboxylate with $LiAlH_4$	
Chemical Formula: $C_{18}H_{31}NO_2$	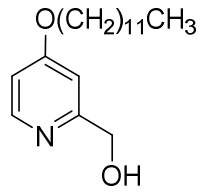
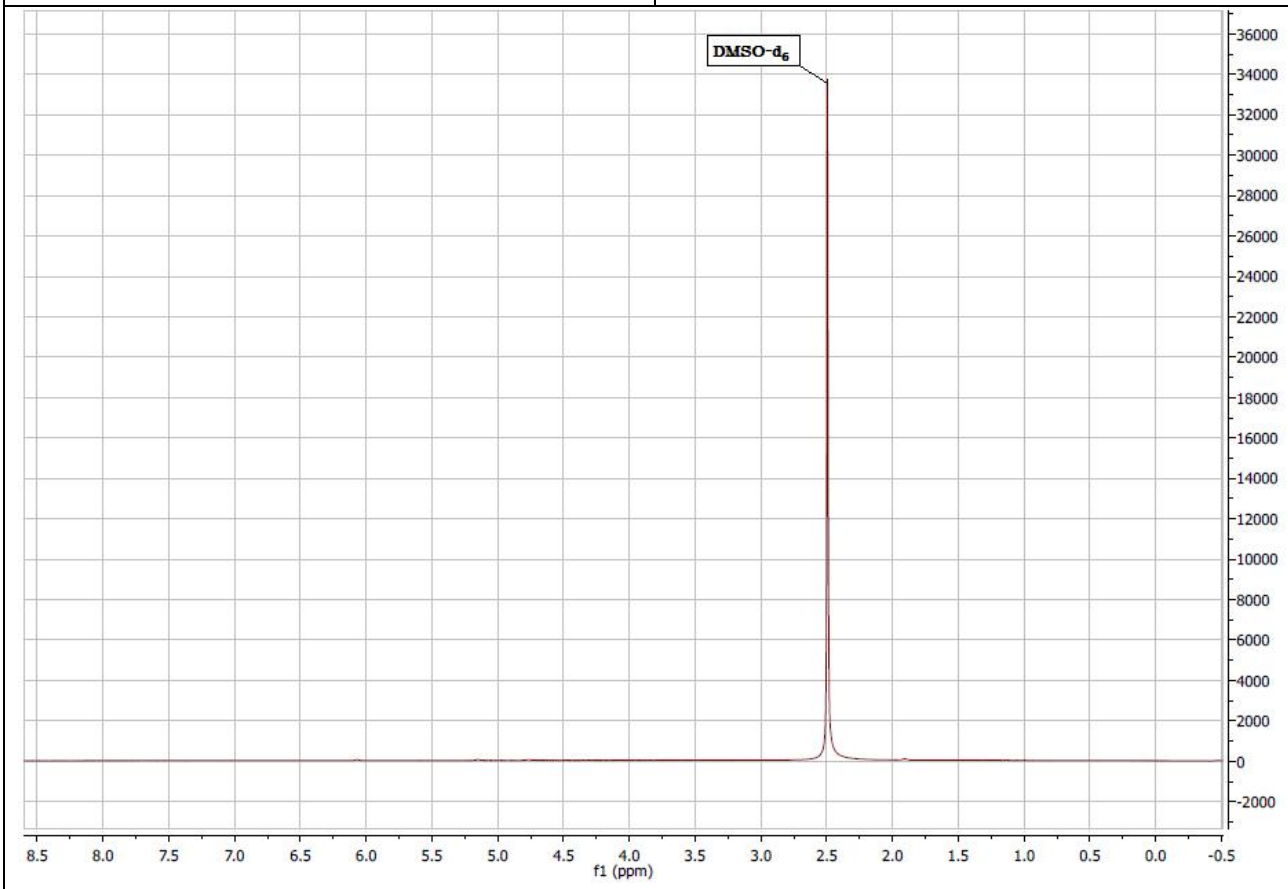	
^{1}H NMR (400 MHz, DMSO-d_6) δ ppm.	

Table 5. ^{1}H NMR of **7f** after attempted reduction with $NaBH_4$ (synthesis 2.1.2f).

^{1}H NMR of 2.1.2f Second attempted reduction of (bcdpmcn)	
Chemical Formula: $C_{18}H_{31}NO_2$	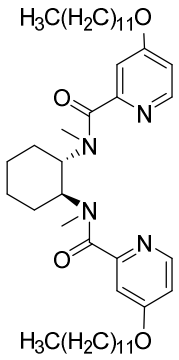

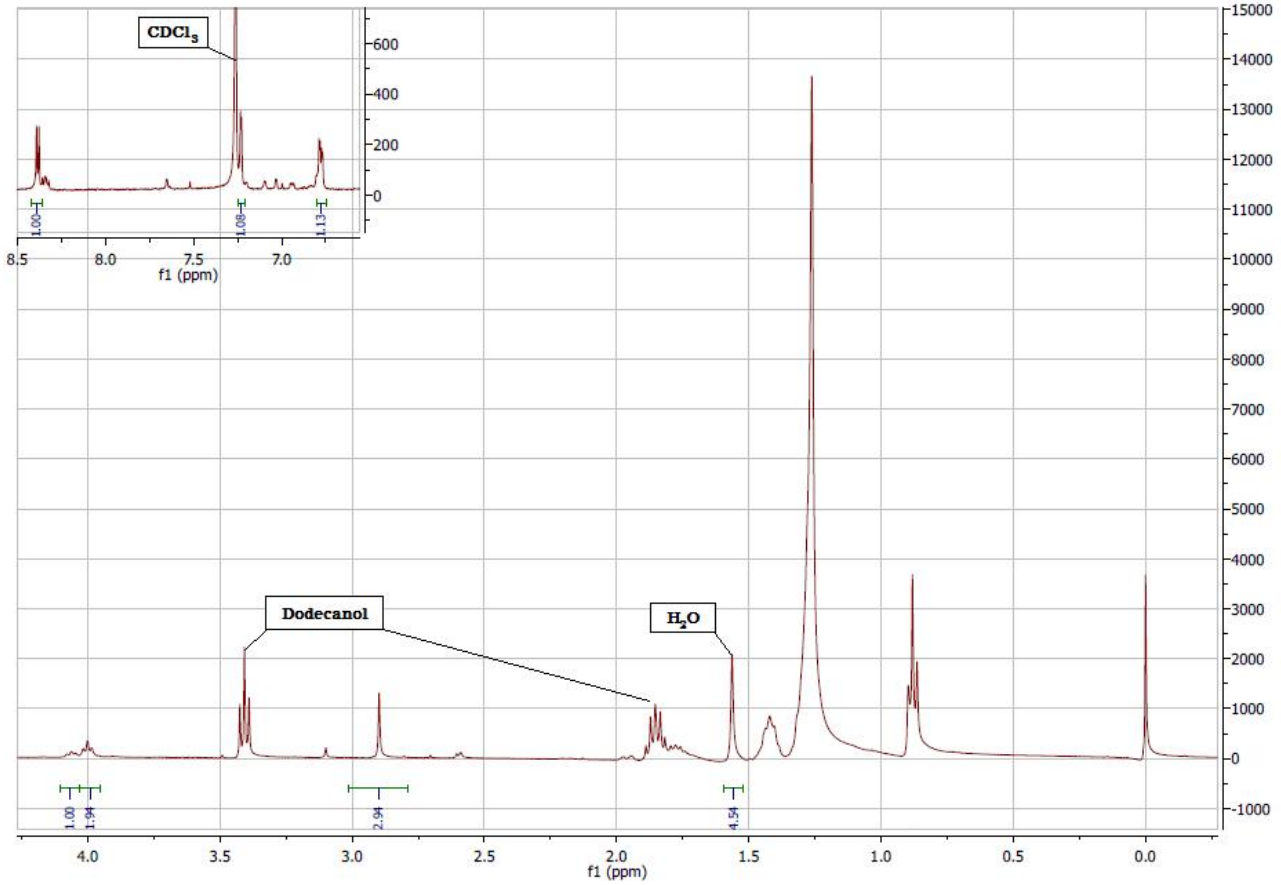

^{1}H NMR (400 MHz, chloroform-d) δ ppm 0.88 (t, 3 H) 1.25 (br s, 14 H) 1.4 (p, 2 H) 1.75 (q, 2 H) 2.85 (s, 3 H) 4.00 (q, 2 H) 4.15 (t, 2 H) 6.52 (dd, 1 H) 7.24 (ds, 1 H) 8.45 (d, 1 H).

(During synthesis 2.1.2a, dodecanol had formed as a byproduct and was thought of to be removed later during final workup).

Table 6. [1]HNMR of product mixture from alkylation of **8a** (synthesis 2.1.3a).

[1]H NMR of 2.1.3a First attempted synthesis of $[Fe(bpdcn)]^{2+}$

8b Chemical Formula: $C_{30}H_{62}N_2$
8c Chemical Formula: $C_{18}H_{38}N_2$
8d Chemical Formula: $C_{42}H_{86}N_2$

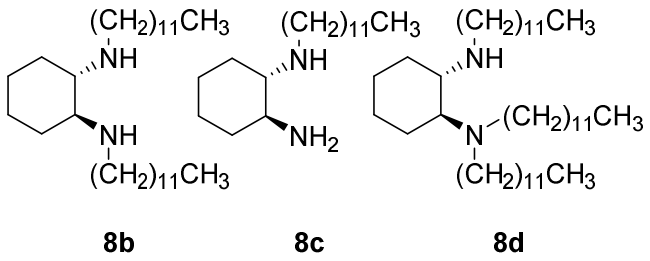

8b **8c** **8d**

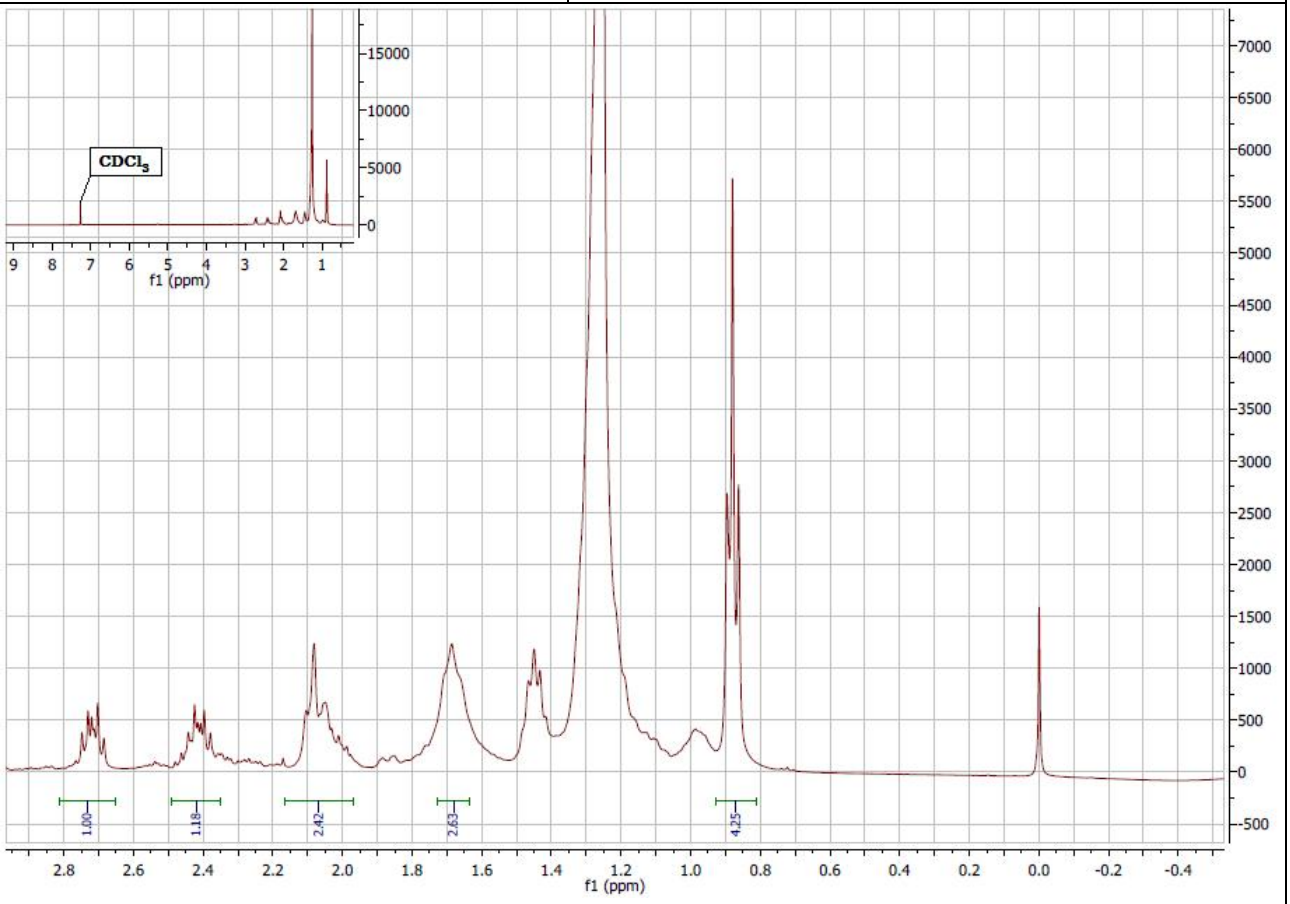

[1]H NMR (400 MHz, chloroform-d) δ ppm 0.88 (t, 3 H) 0.93 (m, 2 H) 1.27 (br s, 38 H) 1.45 (p, 2 H) 1.68 (m, 2 H) 2.09 (m, 2 H) 2.42 (m, 1 H) 2.75 (m, 1 H).

(As a lot of protons on the carbon chains overlap it is hard to distinguish the three compounds **8b**, **8c** and **8d** from one another).

Table 7. [1]HNMR of ligand product **8j** (synthesis 2.1.3d)

[1]H NMR of ligand 8j from synthesis 2.1.3d	
Chemical Formula: $C_{42}H_{72}N_4$	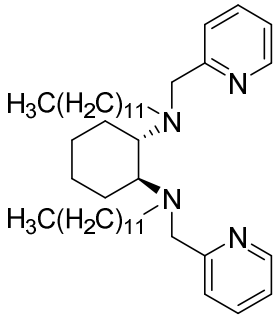
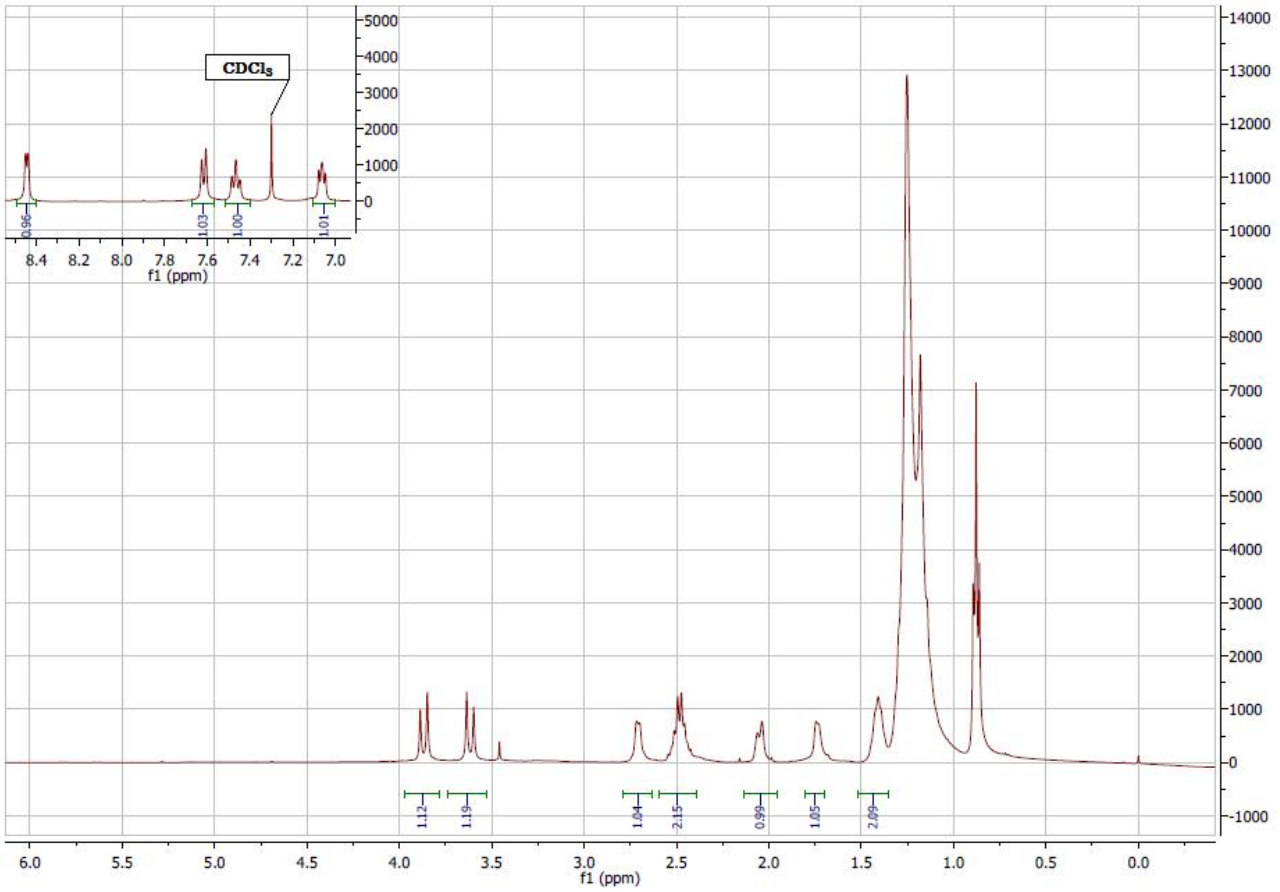	
[1]H NMR (400 MHz, chloroform-d) δ ppm 0.88 (t, 3 H) 1.23 (br s, 16 H) 1.4 (m, 2 H) 1.75 (m, 1 H) 2.1 (m, 1 H) 2.5 (m, 2 H) 2.42 (m, 1 H) 2.75 (m, 1 H) 3.6 (d, 1 H) 3.8 (d 1 H) 7.05 (td, 1 H) 7.45 (td, 1 H) 7.6 (dd, 1 H) 8.45 (dd, 1 H).	

HPLC chromatograms and MS spectra

Table 8. HPLC chromatogram and MS spectrum of product from reaction 2.1.2c.

Chromatogram and mass spectrum of product from reaction 2.1.2c.
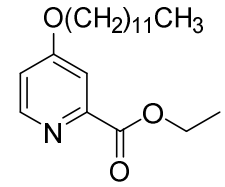 m/z: 336
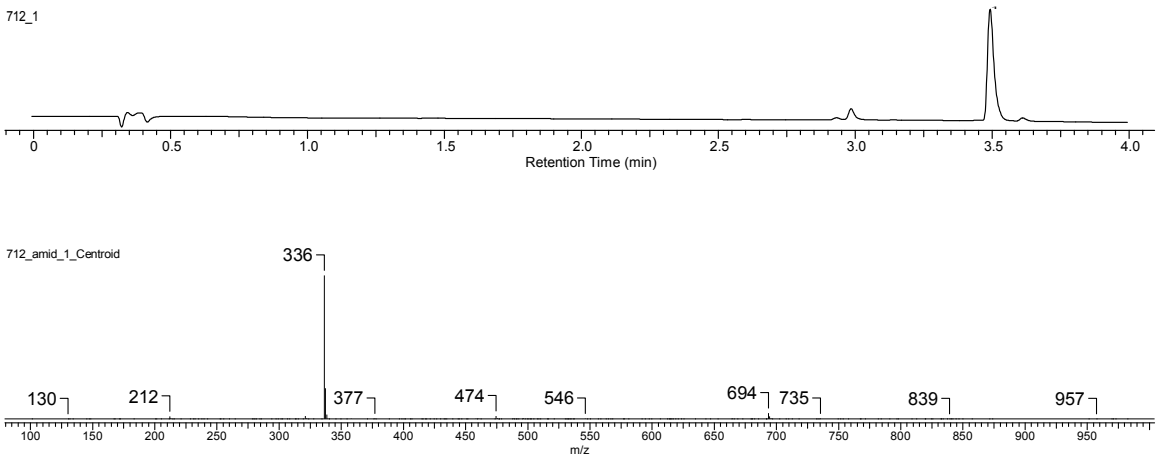
ESI-MS: *m/z* 336.25 [M+H$^+$] (100%)

Table 9. HPLC chromatogram and MS spectra of product mixture from reaction 2.1.2c

Chromatogram and mass spectrum for product mixture from reaction 2.1.2c.
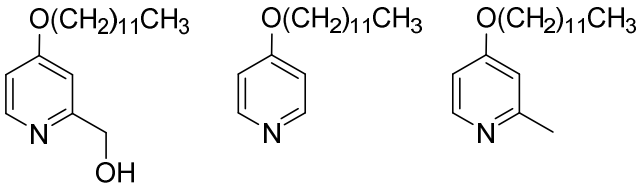 m/z: 294 m/z: 264 m/z: 278
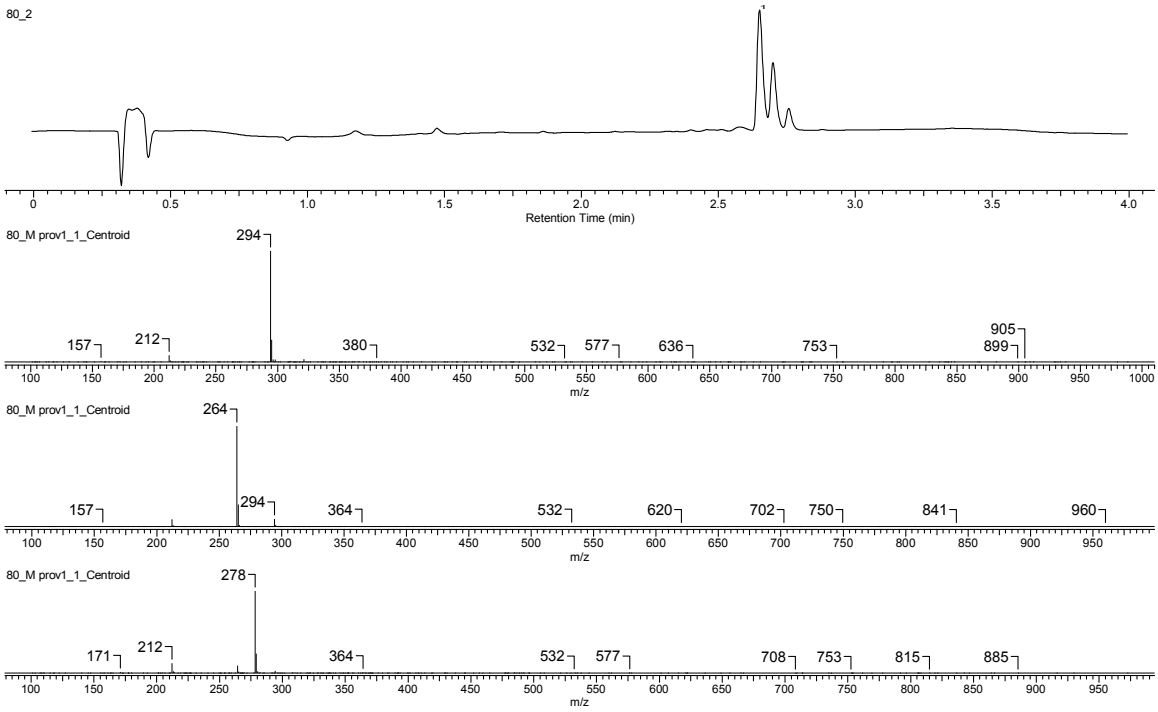
ESI-MS: *m/z* 294.26 [M+H$^+$] (70%) 264 [M+H$^+$] (25%) 278 [M+H$^+$] (5%).

Table 10. HPLC chromatogram and MS spectra of product mixture from reaction 2.1.2e.

Chromatogram and mass spectrum for product mixture from reaction 2.1.2e.
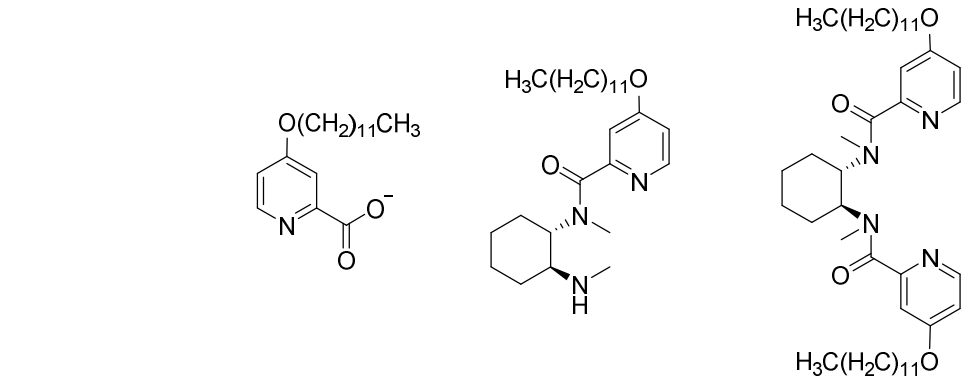 m/z: 308 m/z: 432 m/z: 722
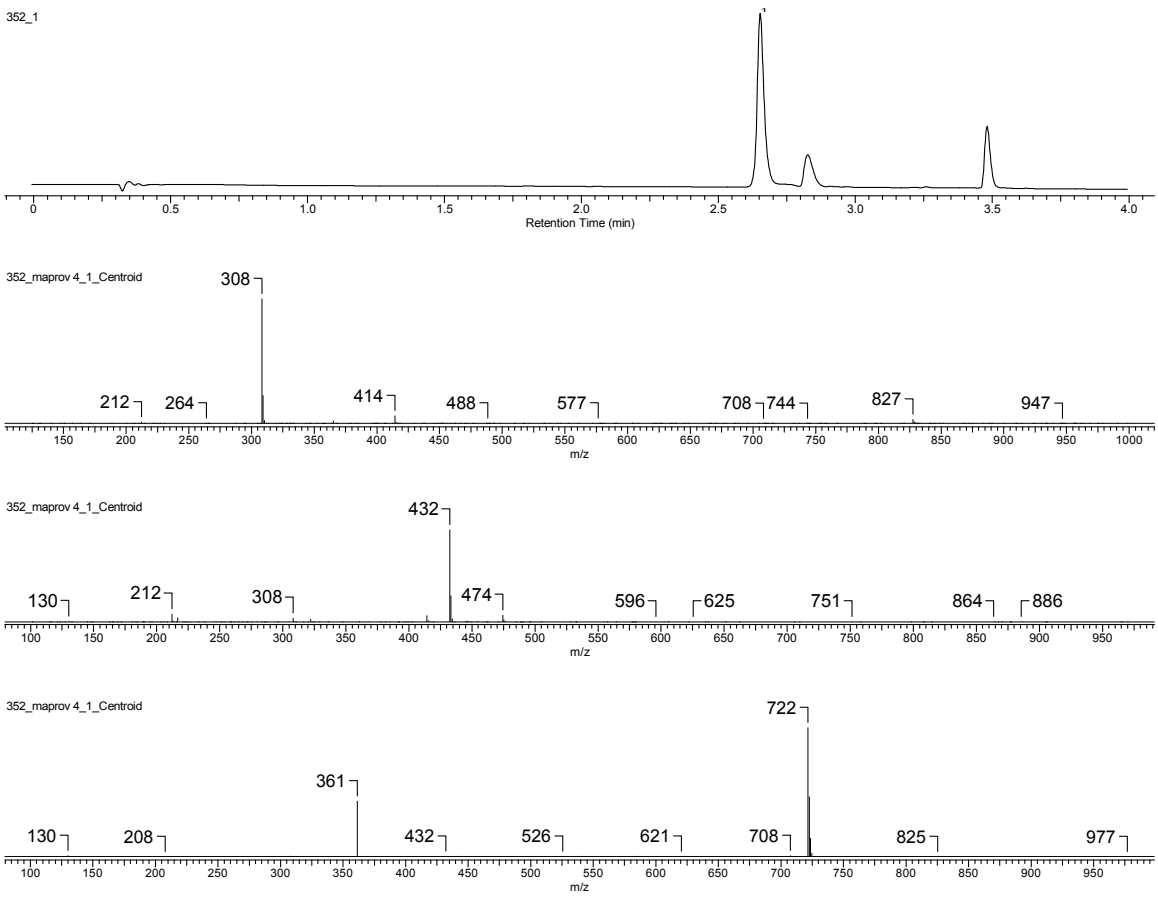
ESI-MS: *m/z* 308 [M+H$^+$] (53%), 432 [M+H$^+$] (27%), 722 [M+H$^+$] (15%), 361 [M+H$^+$] 5%.

Table 11. HPLC chromatogram and MS spectra of product mixture from reaction 2.1.2f.

Chromatogram and mass spectrum for product mixture from reaction 2.1.2f.
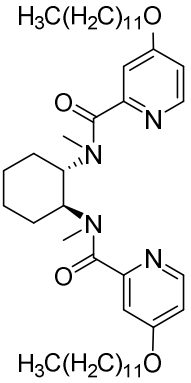
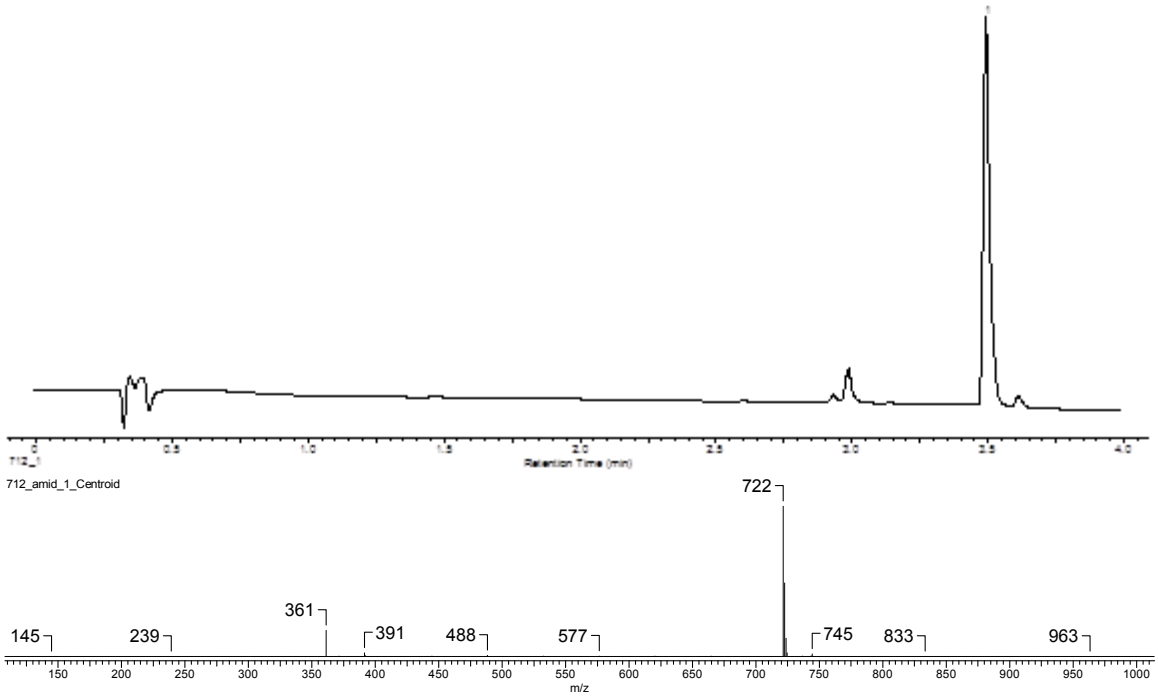
ESI-MS: *m/z* 722 [M+H$^+$] (90%), 361 [M+2H$^+$] (10%).

Table 12. HPLC chromatogram and MS spectra of product mixture from reaction 2.1.3a.

Chromatogram and mass spectrum for product mixture from reaction 2.1.3a.
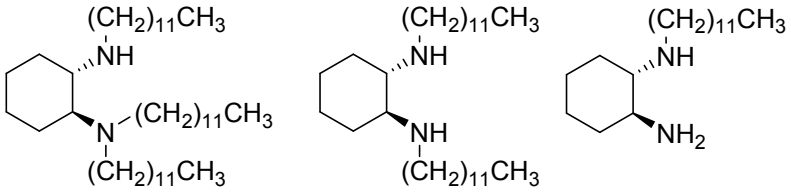 m/z: 618 m/z: 452 m/z: 283
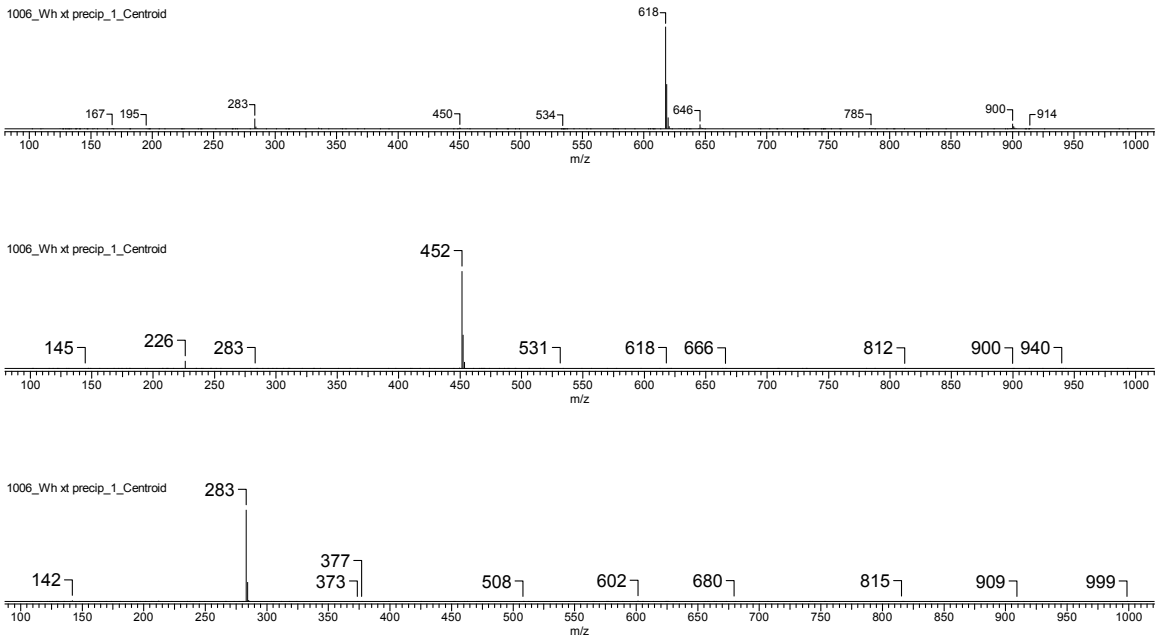
ESI-MS: *m/z* 618 [M+H$^+$] 452 [M+H$^+$] 283 [M+H$^+$]. As product doesn't absorb UV light, the chromatogram is not available and quantification not possible.

Table 13. HPLC chromatogram and MS spectra of product mixture from reaction 2.1.3b.

Chromatogram and mass spectrum for product mixture from reaction 2.1.3b.
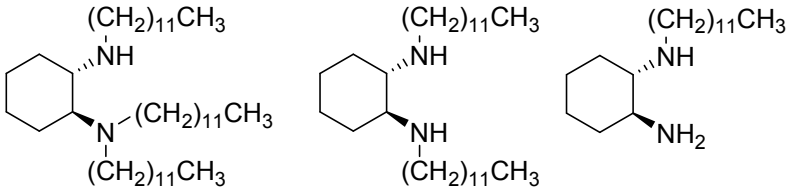 m/z: 618 m/z: 452 m/z: 283
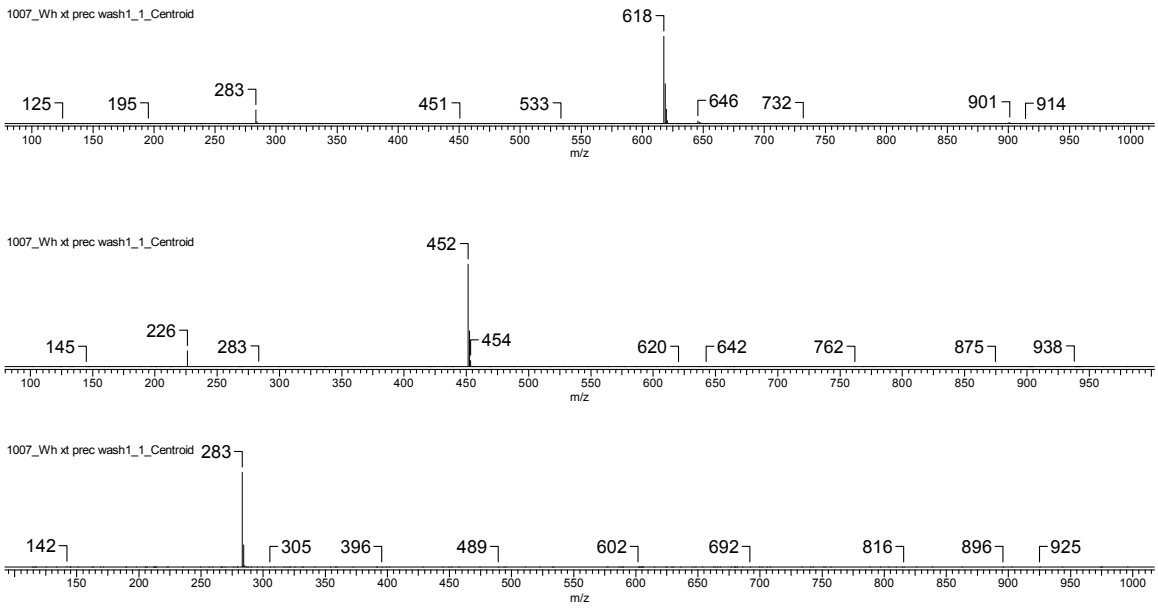
ESI-MS: *m/z* 618 [M+H$^+$] 452 [M+H$^+$] 283 [M+H$^+$]. As product doesn't absorb UV light, the chromatogram is not available and quantification not possible.

Table 14. HPLC chromatogram and MS spectra of product mixture from reaction 2.1.3c.

Chromatogram and mass spectrum for product mixture from reaction 2.1.3c.
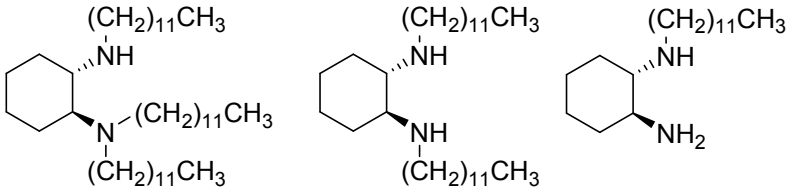 m/z: 618 m/z: 452 m/z: 283
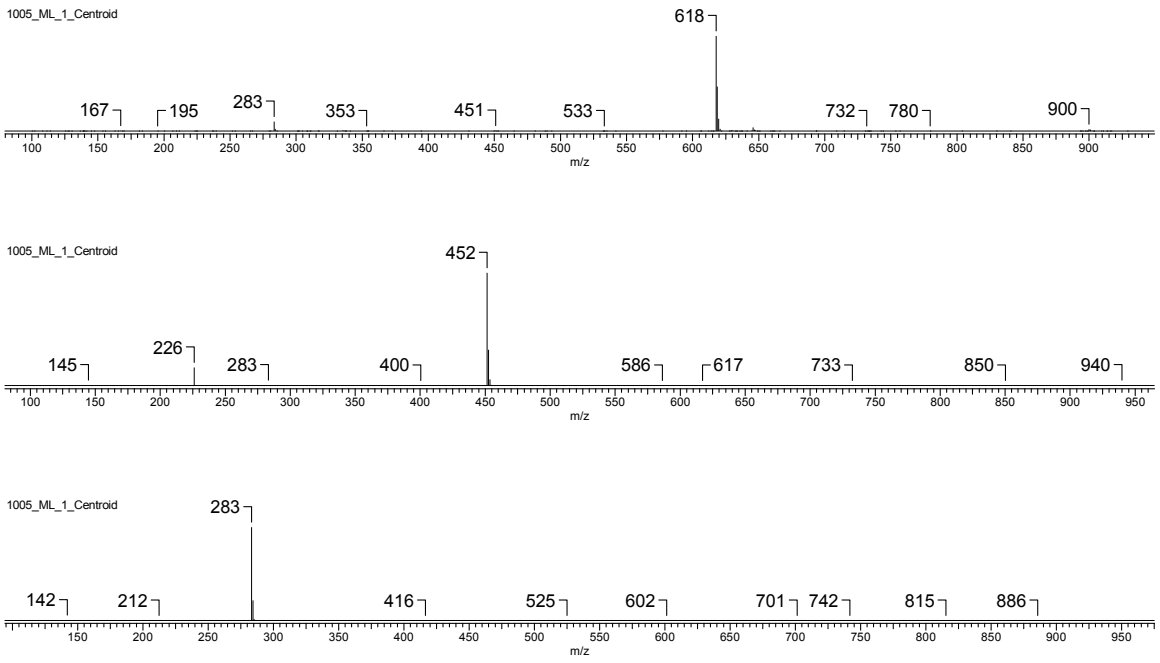
ESI-MS: *m/z* 618 [M+H$^+$] 452 [M+H$^+$] 283 [M+H$^+$]. As product doesn't absorb UV light, the chromatogram is not available and quantification not possible.

Table 15. HPLC chromatogram and MS spectra of product mixture from reaction 2.1.3d.

Chromatogram and mass spectrum for product mixture from reaction 2.1.3d.
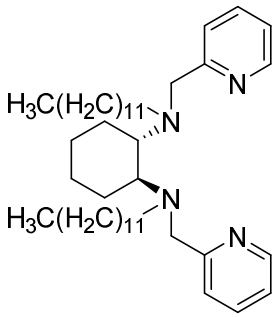 m/z: 634
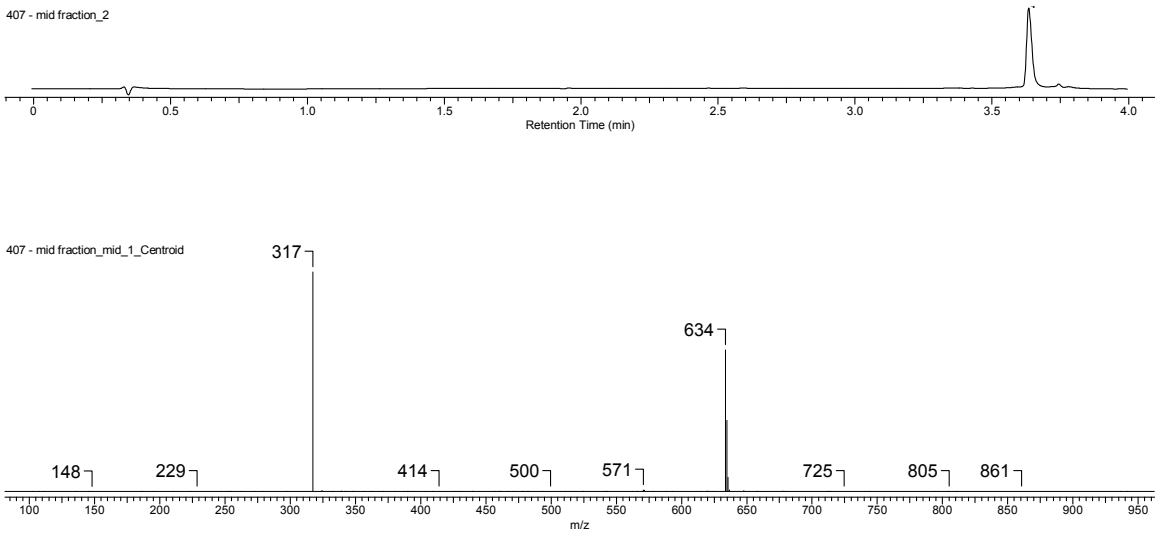
ESI-MS: *m/z* 634 [M+H$^+$], 317 [M+2H$^+$]

Solvents and solvent systems

Table 16. Tested solvents for ^{1}H NMR measurements of **6.**

Solvent	Acetone-d_6	Acetonitrile-d_3	Chloroform-d	Dimethyl sulfide-d_6	Deuterium oxide	Methanol-d_4
Ability to dissolve 6	No	No	Yes	Yes	Yes	Yes
^{1}H NMR active	No	No	No	No	No	No

Table 17. Systems of eluents tested with TLC for purification of **8b**.

Stationary phase	Eluent	Ratios	Separation
Silica gel	DCM/Methanol	95:5	No
Silica gel	DCM/Methanol	90:10	No
Silica gel	EtOAc/Heptane	20:80	No
Silica gel	EtOAc/Heptane	50:50	No
Silica gel	DCM/Methanol/Et_3N	95:5:1	No
Silica gel	DCM/Methanol/NH_4OH	95:5:1	No
Silica gel	DCM/Methanol/Et_3N	90:10:1	No
Silica gel	DCM/Methanol/NH_4OH	90:10:1	No
Silica gel	DCM/Methanol/NH_4OH	50:50:1	No
Silica gel	Diethyl ether/EtOAc	50:50:1	No
Silica gel	EtOAc/Methanol/Et_3N	50:50:1	No
Silica gel	EtOAc/Heptane/Et_3N	20:80:1	No
Silica gel	DCM/Heptane/Et_3N	70:30:1	No
Silica gel	DCM/Petroleum ether/Et_3N	70:30:1	No
Aluminum oxide	DCM/Methanol	95:5	No
Aluminum oxide	DCM/Methanol	90:10	No
Aluminum oxide	EtOAc/Heptane	20:80	No
Aluminum oxide	EtOAc/Heptane	50:50	No
Aluminum oxide	DCM/Methanol/Et_3N	95:5:1	No
Aluminum oxide	DCM/Methanol/NH_4OH	95:5:1	No
Aluminum oxide	DCM/Methanol/Et_3N	90:10:1	No
Aluminum oxide	DCM/Methanol/NH_4OH	90:10:1	No
Aluminum oxide	DCM/Methanol/NH_4OH	50:50:1	No
Aluminum oxide	Diethyl ether/EtOAc	50:50:1	No
Aluminum oxide	EtOAc/Methanol/Et_3N	50:50:1	No
Aluminum oxide	EtOAc/Heptane/Et_3N	20:80:1	No
Aluminum oxide	DCM/Heptane/Et_3N	70:30:1	No
Aluminum oxide	DCM/Petroleum ether/Et_3N	70:30:1	No
RP C8	H_2O/Acetonitrile	Grad 5-90%	Yes

References

[1] J. H. Alstrum-Acevedo, M. K. Brennaman, T. J. Meyer, Inorg. Chem. 2005, 44, 6802-6827.

[2] PhD Thesis by Lele Duan, "Artificial Water Splitting: Ruthenium Complexes for Water Oxidation", (ISBN: 978-91-7501-083-0).

[3] J. Bassham, A. Benson, M. Calvin, J Biol Chem 1950, 185 (2): 7817

[4] Kok, B., B. Forbush, and M. McGloin. 1970. Cooperation of charges in photosynthetic O2 evolution. I. A linear four-step mechanism. Photochem. Photobiol. 11:467–475.

[5] Y. Umena, K. Kawakami, J.-R. Shen, N. Kamiya, Nature 2011, 473, 55-60

[6] A. Zouni, H.-T. Witt, J. Kern, P. Fromme, N. Krauss, W. Saenger, P. Orth, Nature 2001, 409, 739-743.

[7] K. N. Ferreira, T. M. Iverson, K. Maghlaoui, J. Barber, S. Iwata, Science 2004, 303, 1831-1838

[8] B. Loll, J. Kern, W. Saenger, A. Zouni, J. Biesiadka, Nature 2005, 438, 1040-1044.

[9] J. Limburg, J. S. Vrettos, L. M. Liable-Sands, A. L. Rheingold, R. H. Crabtree, G. W. Brudvig, Science 1999, 283, 1524-1527.

[10] M. Yagi, K. Narita, J. Am. Chem. Soc. 2004,126, 8084-8085.

[11] G. C. Dismukes, R. Brimblecombe, G. A. N. Felton, R. S. Pryadun, J. E. Sheats, L. Spiccia, G. F. Swiegers, Acc. Chem. Res. 2009, 42, 1935-1943.

[12] S. W. Gersten, G. J. Samuels, T. J. Meyer, J. Am. Chem. Soc.1982,104, 4029-4030.

[13] Lei Wang, Lele Duan, Ying Wang, Mårten S. G. Ahlquist and Licheng Sun*, Chem**.** Commun**.**, 2014,50, 12947-12950

[14] Emsley, J. (2003). "Ruthenium". *Nature's Building Blocks: An A-Z Guide to the Elements*. Oxford, England, UK: Oxford University Press. pp. 368–370. ISBN 0-19-850340-7.

[15] N. D. McDaniel, F. J. Coughlin, L. L. Tinker, S. Bernhard, J. Am. Chem. Soc.2008,130,210-217.

[16] J. F. Hull, D. Balcells, J. D. Blakemore, C. D. Incarvito, O. Eisenstein, G. W. Brudvig, R. H.Crabtree,J. Am. Chem. Soc. 2009 131, 8730-8731.

[17] J. D. Blakemore, N. D. Schley, D. Balcells, J. F. Hull, G. W. Olack, C. D. Incarvito, O. Eisenstein, G. W. Brudvig, R. H. Crabtree, J. Am. Chem. Soc. 2010, 132, 16017-16029.

[18] J. D. Blakemore, N. D. Schley, D. Balcells, J. F. Hull, G. W. Olack, C. D. Incarvito, O. Eisenstein, G. W. Brudvig, R. H. Crabtree, J. Am. Chem. Soc. 2010, 132, 16017-16029.

[19] Q. Yin, J. M. Tan, C. Besson, Y. V. Geletii, D. G. Musaev, A. E. Kuznetsov, Z. Luo, K. I. Hardcastle, C. L. Hill, Science 2010,328, 342-345.

[20] D. J. Wasylenko, C. Ganesamoorthy, J. Borau-Garcia, C. P. Berlinguette, Chem. Commun. 2011, 47, 4249-4251.

[21] D. K. Dogutan, R. McGuire, D. G. Nocera, J. Am. Chem. Soc. 2011, 133, 9178-9180

[22] Javier Jesus Concepcion Corbea, Zuofeng Chen, Jonah Wesley Jurss, Joseph L. Templeton, Paul Hoertz, Thomas J. Meyer," Ruthenium or osmium complexes and their uses as catalysts for water oxidation", U.S. Patent 8524903 B2, 3 September 2013.

[23] Teng Zhang, Cheng Wang, Shubin Liu, Jin-Liang Wang, Wenbin Lin, J. Am. Chem. Soc., 2014, 136 (1), pp 273–281.

[24] Shoshanna M. Barnett, Karen I. Goldberg, James M. Mayer, Nature Chemistry 2012, 4, 498–502.

[25] W. C. Ellis, N. D. McDaniel, S. Bernhard, T. J. Collins, J. Am. Chem. Soc. 2010, 132, 10990-10991.

[26] A. J. Bard and M. A. Fox, Acc. Chem. Res. 1995, 28, 141–145

[27] J. Chow, R. J. Kopp and P. R. Portney, Science2003,302,1528–1531

[28] T. N. Verziroglu and F. Barbir, Int. J. Hydrogen Energy 1992, 17, 391–404

[29] N. S. Lewis, Nature2001, 414,589–590

[30] Altork, L.N. & Busby, J. R. (2010 Oct). Hydrogen fuel cells: part of the solution. Technology & Engineering Teacher, 70(2), 22-27.

[31] Zehner, Ozzie (2012). *Green Illusions*. Lincoln and London: University of Nebraska Press. pp. 1–169, 331–42

[32] Häussinger, Peter; Lohmüller, Reiner; Watson, Allan M. (2011). "Hydrogen, 1. Properties and Occurrence". *Ullmann's Encyclopedia of Industrial Chemistry*.

[33] http://energy.gov/eere/fuelcells/hydrogen-production, U.S. Department of Energy. 2008-12-15.
[34]PhD Thesis by Aida Rodrigues, "The effects of Carbon Monoxide Contamination on Proton-Exchange Membrane Fuel cells", (ISBN: 0-7803-4515-0).
[35] von Hofmann, A. W. *Introduction to Modern Chemistry: Experimental and Theoretic; Embodying Twelve Lectures Delivered in the Royal College of Chemistry, London*. Walton and Maberly, London, **1866**.
[36] Marie-Cécile Pera, Daniel Hissel, Hamid Gualous, Christophe Turpin John Wiley & Sons, (2013). "Electrochemical Components". ISTE Wiley.
[37] Carmo, M, Fritz D, Mergel J, Stolten D, (2013). "A comprehensive review on PEM water electrolysis". Journal of Hydrogen Energy.
[38] Aaron K. Vannuccia, Leila Alibabaeia, Mark D. Losegob, Javier J. Concepciona, Berç Kalanyanb, Gregory N. Parsonsb,and Thomas J. Meyer, PNAS, 2013, vol. 110 no. 52, 20918–20922.

[39] Benjamin M. Klepser and Bart M. Bartlett* J. Am. Chem. Soc. 2014, 136, 1694−1697
[40] Joshua R. Dunetz,*,† Yanqiao Xiang,‡ Aaron Baldwin,‡ and Justin Ringling‡ Org. Lett., Vol. 13, No. 19, 201, 5048-5051.
[41] Kahn, O.Molecular Magnetism; VCH: New York, 1993.

[42] Tsung-Hsien Ho, Chien-Chen Lai, Yi-Hung Liu, Shie-Ming Peng, and Sheng-Hsien Chiu* Chemistry - A European Journal, 2014, 4563-4567;

[43] Schweiger, A. and Jeschke, G. (2001). *Principles of pulse electron paramagnetic resonance*. Oxford, UK: Oxford University Press.
[44] J. Justing Goodling Electrochimica Acta 50 (2005), 3049-3060.